Carbonate crash and biogenic bloom in the late Miocene: Evidence from ODP Sites 1085, 1086, and 1087 in the Cape Basin, southeast Atlantic Ocean

L. Diester-Haass

Zentrum für Umweltwissenschaften der Universität, Universität des Saarlandes, Saarbrücken, Germany

P. A. Meyers

Marine Geology and Geochemistry Program, Department of Geological Sciences, University of Michigan, Ann Arbor, Michigan, USA

T. Bickert

Fachbereich Geowissenschaften, Universität Bremen, Bremen, Germany

Received 26 May 2003; revised 6 October 2003; accepted 31 October 2003; published 4 February 2004.

[1] Middle/late Miocene to early Pliocene sedimentary sequences along the continental margin of southwest Africa have changes that correspond to the carbonate crash (12–9 Ma) and biogenic bloom events (~7–4 Ma) described in the equatorial Pacific by *Farrell et al.* [1995]. To explore the origins of these changes, we analyzed the carbon and coarse fraction contents of sediments from ODP Sites 1085, 1086, and 1087 at a time resolution of 5 to 30 kyr. Several major drops in $CaCO_3$ concentration between 12 and 9 Ma are caused by dilution from major increases in clastic input from the Oranje River during global sea level regressions. Abundant pyrite crystals and good preservation of fish debris reflect low oxygenation of bottom/pore waters. Regional productivity was enhanced during the time equivalent to the carbonate crash period. Higher benthic/planktic foraminiferal ratios indicate that $CaCO_3$ dissolution at Site 1085 peaked between 9 to 7 Ma, which was after the global carbonate crash. This period of enhanced dissolution suggests that Site 1085 was located within a low-oxygen water mass that dissolved $CaCO_3$ more easily than North Atlantic Deep Water, which began to bathe this site at 7 Ma. At 7 to 6 Ma, the onset of the biogenic bloom, increases and variations in total organic carbon and benthic foraminiferal accumulation rates show that paleoproductivity increased significantly above values observed during the carbonate crash period and fluctuated widely. We attribute the late Miocene paleoproductivity increase off southwest Africa to ocean-wide increases in nutrient supply and delivery[1]. *INDEX TERMS:* 3022 Marine Geology and Geophysics: Marine sediments—processes and transport; 4267 Oceanography: General: Paleoceanography; 4279 Oceanography: General: Upwelling and convergences; *KEYWORDS:* $CaCO_3$ MAR, TOC MAR, benthic foraminifers, oxygen isotopes, pyrite, fish debris

Citation: Diester-Haass, L., P. A. Meyers, and T. Bickert (2004), Carbonate crash and biogenic bloom in the late Miocene: Evidence from ODP Sites 1085, 1086, and 1087 in the Cape Basin, southeast Atlantic Ocean, *Paleoceanography*, *19*, PA1007, doi:10.1029/2003PA000933.

1. Introduction

[2] Major changes occurred in the ocean-continent climate system in the middle to late Miocene. Antarctic ice sheets expanded, sea level fluctuated, surface and deep water masses cooled, equator-pole temperature gradients steepened, uplift of the Isthmus of Panama started, silica fractionation between Atlantic and Pacific Oceans developed, C_4 plants expanded, and Himalaya uplift initiated important changes in atmospheric circulation and continental weathering [cf. *Zachos et al.*, 2001].

[3] Within this time interval there are two especially remarkable paleoceanographic events. The first is the "carbonate crash," which was a period between about 12 to 9 Ma when several sharp drops in $CaCO_3$ concentration occurred in the equatorial latitudes of the Pacific and Indian Oceans [*Peterson et al.*, 1992; *Berger et al.*, 1993; *Farrell et al.*, 1995; *Lyle et al.*, 1995; *Lyle*, 2003] and in the Caribbean Sea [*Roth et al.*, 2000]. Changes in deep water circulation, shoaling of the CCD, and shallow-deep fractionation are considered as possible causes. The second event is the "biogenic bloom," which was a significant increase in marine biological productivity that began after 7 Ma and continued into the Pliocene in the equatorial Pacific Ocean [*Farrell et al.*, 1995; *Berger et*

0883-8305/04/2003PA000933

[1]Auxiliary data are available electronically at World Data Center-A for Paleoclimatology, NOAA/NGDC, 325 Broadway, Boulder, CO 80303, USA. (paleo@mail.ngdc.noaa.gov; URL: http://www.ngdc.noaa.gov/paleo)

al., 1993], in the equatorial Atlantic Ocean [*Murray and Peterson*, 1997], and in the Indian Ocean [*Vincent et al.*, 1985; *Peterson et al.*, 1992; *Gupta and Thomas*, 1999; *Dickens and Owen*, 1999], and appears to have started as early as 9 Ma in the southwest Pacific Ocean [*Grant and Dickens*, 2002].

[4] The causes of the carbonate crash and the biogenic bloom remain poorly understood. Here we report multiproxy evidence for these events from three ODP sites that describe a depth transect across the continental margin of southwest Africa, and we provide observations and interpretations that should improve understanding of these events. Our results also add new details to the history of upwelling associated with the Benguela Current.

2. Background

2.1. Study Area

[5] The Benguela Current is the eastern boundary current of the South Atlantic subtropical gyre [*Peterson and Stramma*, 1991]. Southerly and southeasterly trade winds drive coastal upwelling of cold, nutrient rich water from depths of 200–300 m [*Hart and Currie*, 1960] over most of the continental shelf. The cool waters are separated from the warmer subtropical waters of the offshore Atlantic by a thermal front. However, plumes and filaments of upwelled water extend westward and transport nutrients to the open ocean [*Lutjeharms and Stockton*, 1987; *Summerhayes et al.*, 1995]. Phosphate and silica are relatively low in subsurface waters in the Cape Province south of the Benguela Upwelling Area, and productivity is less than in the Namibia Upwelling Area [*Berger et al.*, 2002]. Nearby land areas are dominated by the very dry Namib Desert. The only perennial river is the Oranje River whose sediment load is transported to the shelf and slope and distributed southward by the south-flowing counter currents [*Rogers and Bremner*, 1991; *Summerhayes et al.*, 1995].

[6] Previous investigations of the Miocene history of upwelling off southwest Africa concluded that the onset of high productivity was at about 10 Ma (see the *Berggren and Kent* [1985] timescale) [*Siesser*, 1980; *Meyers et al.*, 1983] and postulated that the Benguela Current and related upwelling migrated progressively from south to north within the late Miocene and Pliocene [*Diester-Haass et al.*, 1990, 1992]. These early interpretations were hampered by incomplete sediment sequences, poor temporal resolution, and information from only one location - DSDP Site 362/532 on the Walvis Ridge [*Bolli et al.*, 1978; *Hay et al.*, 1984; *Hay and Brock*, 1992; *Diester-Haass et al.*, 1990, 1992].

[7] ODP Leg 175 recovered continuous sediment sequences from multiple sites that greatly expand opportunities to study the history of the Benguela Current Upwelling System. *Lange et al.* [1999], *Marlow et al.* [2000], *Christensen et al.* [2002], *Giraudeau et al.* [2002], and *Robinson and Meyers* [2002] describe Pleistocene-Pliocene portions of Benguela Current upwelling history. Our investigation focuses on the early Pliocene to middle-late Miocene period at Sites 1085, 1086, and 1087 in the Cape Basin. The three ODP sites form a depth transect across the upper continental slope of southwest Africa (Figure 1). Site 1085 (1713 m water depth) is at the outer rim of the Oranje River fan, where the shelf is relatively wide (180 km) [*Shannon and Nelson*, 1996]. Sites 1086 (781 m water depth) and 1087 (1371 m water depth) are located on the narrower continental slope off South Africa [*Wefer et al.*, 1998a].

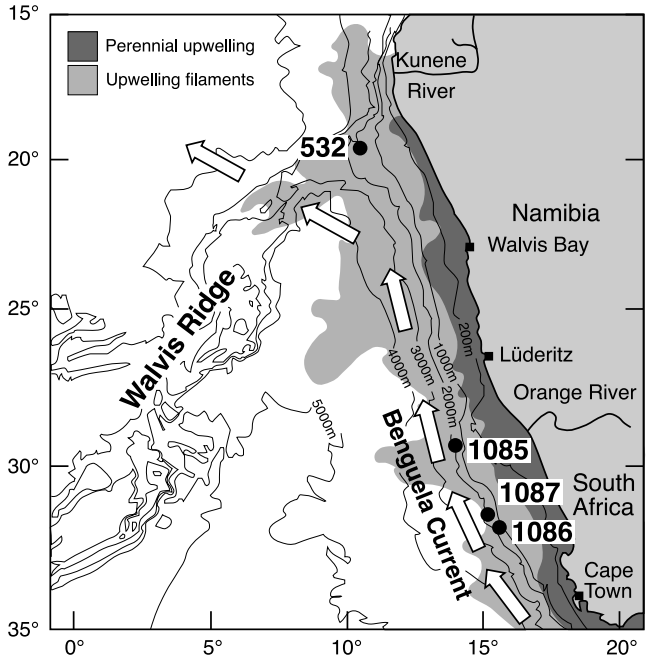

Figure 1. Locations of ODP Sites 1086 (781 m), 1087 (1371 m), and 1085 (1713 m), which form a depth transect on the continental slope of the Cape Basin and DSDP Site 532/362 (1331 m) on the Walvis Ridge. Shading identifies areas of perennial and periodic upwelling as defined by *Lutjeharms and Stockton* [1987].

2.2. Samples and Analysis

[8] We selected sediment sequences starting in the middle Pliocene and continuing to the Miocene limits that were imposed in Hole 1085A by a slump at 603 meters below seafloor (mbsf) (14.47 Ma), in Hole 1086A by the limit of coring at 205 mbsf (7.5 Ma), and in Hole 1087C by a slump at 424 mbsf (11.57 Ma) [*Wefer et al.*, 1998a]. We obtained 10 cm^3 samples at intervals of 50 to 100 cm, which correspond to time intervals of 5 to 30 kyr depending on sedimentation rates.

[9] Two g of each sample were set aside for carbon analyses, and the remainder was washed through 40 and 63 μm sieves. The >40 μm fraction was used for a combined coarse fraction and isotope analysis. The >63 μm fraction was sieved into 63–125, 125–250, 250–500, and >500 μm fractions. In each fraction, 800 grains (if present) were counted and up to 25 biogenous, terrigenous and authigenous components were identified. The percent composition of the coarse silt (40–63 μm) and sand fraction was calculated by multiplying the percentage of each individual component in each fraction by the weight of the fraction.

[10] Carbon analyses were done on the sediment records from Sites 1085 and 1087 but not on the abbreviated record from Site 1086. Freeze-dried samples of bulk sediment were

analyzed for $CaCO_3$ concentrations using the carbonate bomb technique of *Müller and Gastner* [1971]. Weighed samples were reacted with 3N HCl, and the volume of CO_2 released from each sample was measured and compared to the volumes released from known amounts of pure $CaCO_3$ to determine the percentage (±1%) in the sample. The carbonate-free residue after acid treatment was collected, rinsed, and dried. Amounts of total organic carbon (TOC) in the carbonate-free residues were measured with a Carlo Erba 1108 CHNS analyzer. This procedure involves heating the sample at 1020°C and measuring the combustion products by gas chromatography [*Verardo et al.*, 1990]. TOC concentrations (±0.05%) were calculated on a whole-sediment basis by adjusting for the $CaCO_3$ concentrations determined from the bomb technique.

[11] Determinations of the $\delta^{18}O$ values of shells of the benthic foraminifera *Cibicidoides wuellerstorfi* and *C. kullenbergi* in the >250 μm fraction samples from Hole 1085A were measured using a Finnigan MAT 252 mass spectrometer (T. Westerhold and T. Bickert, Middle to Late Miocene Oxygen Isotope Stratigraphy of ODP Site 1085—SE Atlantic, submitted to *Palaeogeography, Palaeoclimatology, Palaeoecology*, 2003, hereinafter referred to as Westerhold and Bickert, submitted manuscript, 2003). Data are reported in per mil VPDB after calibration with NBS 19. The mean external reproducibility is ±0.07‰ relative to an internal carbonate standard (Solnhofen limestone).

2.3. Analytical Strategies

[12] To investigate the causes and consequences for the carbonate crash and the biogenic bloom events, we employed different suites of proxies to assess carbonate dissolution, carbonate dilution by other sediment components, sea level changes, and paleoproductivity changes.

2.3.1. Evidence of $CaCO_3$ Dissolution

[13] We used the benthic/planktic foraminiferal ratio (B/P), which is calculated as (% benthics/% benthics +% planktics)*100, as a proxy for dissolution to detect variations in content and flux of $CaCO_3$ and to relate them to possible dissolution changes. The B/P ratio is influenced by water depth (which is assumed to have been nearly constant during the investigated period), by-productivity (with increasing export productivity and food supply to the seafloor benthic foraminiferal numbers will increase), and by carbonate dissolution (planktic foraminifers are more easily dissolved than benthic ones [*Parker and Berger*, 1971]). In addition, increased paleoproductivity enhances carbonate dissolution at the seafloor by microbial metabolism of organic matter and consequent CO_2-enhanced calcite dissolution [*Archer and Maier-Reimer*, 1994]. Thus increased paleoproductivity exerts a two-fold effect on the benthic/planktic foraminiferal ratio: it can increase benthic foraminiferal numbers, and it can increase dissolution of planktic foraminifers. Both effects increase the ratio and potentially complicate its interpretation.

[14] Benthic foraminifers, which form the main basis for our reconstruction of paleoproductivity, can also be subject to dissolution. However, lack of strong fragmentation of planktic foraminifers and the observation of parallel increases in accumulation rates of benthic and planktic foraminifers [*Diester-Haass et al.*, 2002] indicate that benthic foraminiferal numbers are not markedly affected by dissolution.

2.3.2. Evidence of $CaCO_3$ Dilution and Sea Level Change

[15] Decreases in carbonate concentration might be caused not only by dissolution of carbonate but also by dilution by other sediment components. We therefore studied the concentrations of terrigenous particles in the >40 μm size fractions, reasoning that silt and sand-sized clastic particles form the coarsest tail of terrigenous input and would consequently be proxies for total clastic delivery and transport energy.

[16] We explored possible relations between the carbonate crash and biogenic bloom events and sea level changes by looking at the abundance of shelf-derived glauconite particles, phosphate grains, worn shell material, and the remains of shallow water organisms such as bryozoans, decapods, and thick-walled molluscan debris. We postulated that these particles might be transported to the continental slope more easily during regressions and seaward migration of the shoreline [*McRae*, 1972; *Rogers and Bremner*, 1991; *Wefer et al.*, 1998a].

2.3.3. Paleoproductivity Estimates

[17] Paleoproductivity reconstructions can be problematic on ocean margins. We therefore used multiple proxies to assess changes in paleoproductivity. Recognizing that carbon accumulation rates are sometimes increased by downslope transport [*Diester-Haass et al.*, 1992; *Sancetta et al.*, 1992; *Summerhayes et al.*, 1995] and can be decreased by dissolution and degradation, we employed concentrations and mass accumulation rates of $CaCO_3$ and TOC. We also made use of the organic matter $\delta^{13}C$ values from Hole 1085A published by *Twichell et al.* [2002]. Because opal production mirrors changes in seawater chemistry along the southwest Africa margin more than the upwelling process itself, the presence of opal has been discontinuous in sediment records of the Benguela Current Upwelling System [*Lange and Berger*, 1993; *Summerhayes et al.*, 1995; *Lange et al.*, 1999; *Berger et al.*, 2002]. We elected not to use this paleoproductivity proxy because of its discontinuous nature.

[18] Benthic foraminiferal concentrations and accumulation rates (BFAR) are valuable proxies for reconstructing changes in export paleoproductivity [*Herguera and Berger*, 1991; *Herguera*, 2000; *Nees*, 1997; *Schmiedl and Mackensen*, 1997; *Yasuda*, 1997; *van der Zwaan et al.*, 1999]. These fauna subsist on the amount and nutritional value of the exported organic matter. To address the problem of downslope transport processes that might enhance the BFAR and by inference carbon delivery, we measured benthic foraminiferal numbers in three grain-size fractions (125–250, 250–500 and >500 μm), reasoning that the coarsest ones are most likely to be autochthonous. In addition, we counted the numbers of the benthic foraminifer genus *Uvigerina*, which reflects high export productivity and high delivery rates of organic matter to the seafloor [e.g., *Schmiedl and Mackensen*, 1997; *Gupta and Thomas*, 1999; *Ohkushi et al.*, 2000; *Berger et al.*, 2002] at Site 1086, which lies within the depth range of this genus.

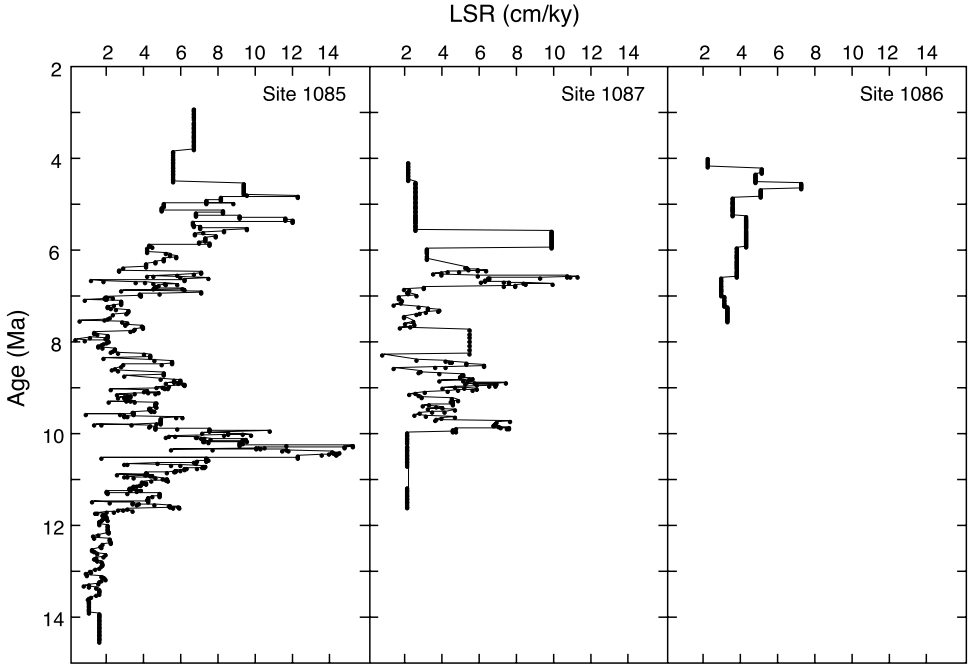

Figure 2. Linear sedimentation rates for ODP Sites 1085 (1713 m), 1087 (1371 m), and 1086 (781 m), obtained from the age model of Westerhold et al. (submitted manuscript, 2003).

2.4. Age Control and Sediment Accumulation Rates

[19] Age models for the Miocene sections of ODP Holes 1085A and 1087C were generated by T. Westerhold et al. (Miocene evolution of carbonate sedimentation in the eastern South Atlantic: High-resolution XRF-scanning records of ODP Sites 1085 and 1087, submitted to *Marine Geology,* 2003, hereinafter referred to as Westerhold et al., submitted manuscript, 2003) using orbital tuning of an XRF_{Fe} intensity record to the summer insolation astronomical solution of *Laskar et al.*, [1993]. Fine-tuning was done iteratively by correlating each prominent maximum of the Fe record to the minima of the target curve. This gave at least one age control point for each eccentricity cycle. Prior to the tuning procedure, a composite record was established by splicing the XRF_{Fe} record of each core from the two holes to the SGR (Magnetic Susceptibility, GRAPE, Reflectance) log of Hole 1085A to compensate for the 10% core-to-core gaps that typify drilled sequences. Shipboard biostratigraphic datums and paleomagnetic measurements provided the preliminary age model for Sites 1085 and 1087 [*Wefer et al.*, 1998a]. Because of coring-induced magnetization, the magnetostratigraphic interpretation at Hole 1085A was only possible down to the bottom of Chron C3n.4n at 5.23 Ma at 280 mbsf depth [*Wefer et al.*, 1998a], therefore precluding a magnetostratigraphic age model for the middle to late Miocene. The age model of Site 1086 is based on shipboard biostratigraphy. A discussion of the age model of *Vidal et al.* [2002] based on the oxygen isotope record and which gave slightly different results especially at the Miocene-Pliocene transition is given in the work of Westerhold et al. (submitted manuscript, 2003).

[20] Linear sedimentation rates (LSR) in Hole 1085A range between 1 and 14 cm/kyr (Figure 2). From 14 Ma up to 10.6 Ma the sedimentation rates were well below 4 cm/kyr. They then steadily increased to a maximum value of 14 cm/kyr at 10 Ma. Thereafter, rates decreased to values below 4 cm/kyr until 6.7 Ma, and then they rose to 6 cm/kyr. In Sites 1086 and 1087, the sedimentation rates range from 5 to 13 cm/kyr and from 2 to 7 cm/kyr, respectively (Figure 2).

[21] We used the improved linear sedimentation rates from our orbital tuning and the sediment porosity and density values available in the work of *Wefer et al.* [1998a] to calculate total sediment mass accumulation rates (MARs). We then calculated individual component MARs for $CaCO_3$ in g/cm^2*kyr, TOC in mg/cm^2*kyr, and benthic foraminifera in number/cm^2*kyr based on the relation:

$$MAR_{component} = (\%\ component/100\ X\ MAR_{bulk\ sediment})$$

3. Results

[22] Concentrations of the sand-sized fraction at the three sites vary between <1% and about 10%, with lower values more common at Site 1085, which is the deepest location (Figure 3). Lowest values appear between 9 and 7 Ma at all sites, and they extend back to 11 Ma during the period of high LSR at Site 1085. The benthic foram $\delta^{18}O$ values from Hole 1085A gradually increase from ~1.7‰ at 14 Ma to about 2.3‰ at10 Ma and then fluctuate between 1.9 and 2.9‰ afterward (Figure 4).

[23] $CaCO_3$ concentrations are generally about 10% lower at Site 1085, which is closer to the Oranje River fan, than at Site 1087 (Figure 5). $CaCO_3$ concentrations drop dramatically between 9.5 and 9 Ma at both sites. Percentages decrease to about 25% at Site 1085 and to about 60% at Site 1087. Several smaller and briefer decreases occur between 12.5 and 10 Ma at Site 1085. $CaCO_3$ MARs change similarly to bulk LSRs at both sites (Figure 6).

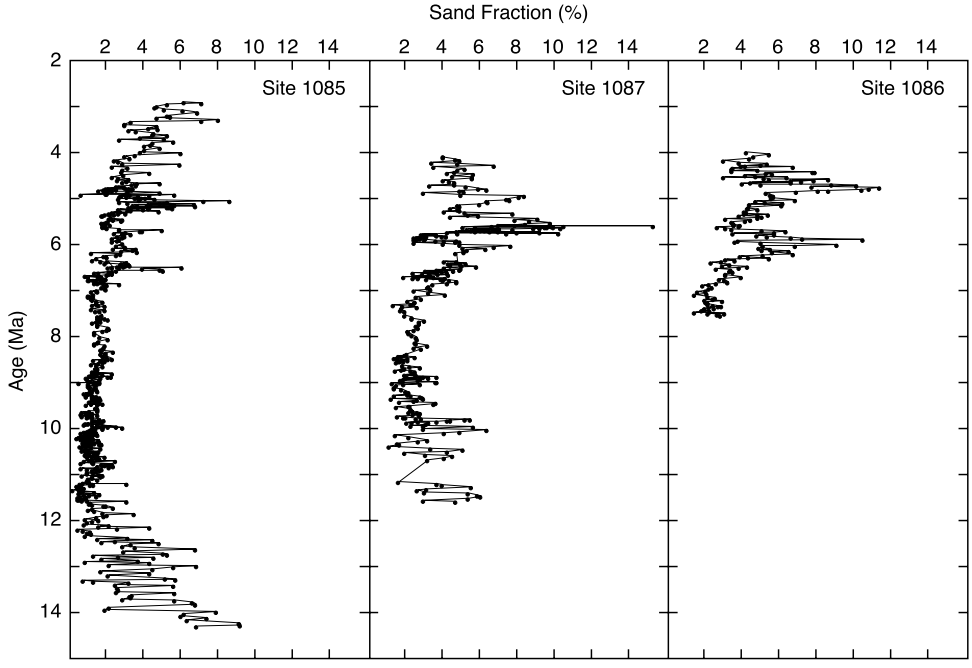

Figure 3. Percent contributions of the sand fraction (>63 μm) to sediments from ODP Sites 1085, 1087, and 1086.

TOC MARs are generally higher at Site 1085 than at Site 1087. The values increase strongly at 6.7 Ma and fluctuate widely thereafter at both sites (Figure 7).

[24] Numbers of benthic foraminifers per gram of sediment (NBF) increase from <300 prior to 8.5 Ma at Sites 1085 and 1087, to exceed 1000 at Sites 1086 and 1087 between 6.5–3 Ma (Figure 8). Values at Site 1087 are similar to or slightly higher than those of Site 1085, whereas maxima at the shallowest Site 1086 are much higher than those at the deeper locations. Changes in the benthic foraminiferal accumulation rates (BFAR) are similar at Sites 1085 and 1087: very low values prior to 11 Ma, higher values from 11 to 9.5 Ma, and a sharp increase at about 7 Ma followed by strong fluctuations (Figure 9). Small foraminifers dominate size distributions at the three sites (Figure 8). Increases in small-sized foraminifers are accompanied by increases in coarse ones, except for two periods at Site 1085, marked by arrows, where small ones increase and coarse ones decrease. Abundances of *Uvigerina spp* at Site 1086 (Figure 10) correlate with variations in NBF and BFAR (Figures 8 and 9). Benthic/planktic foraminiferal ratios are below 10% with small fluctuations prior to 11 Ma. The ratios increase to up to 45% at Site 1085 and 20% at Site 1087 between 9.5 and 7.5 Ma, and then drop to lower but widely fluctuating values after 7.5 Ma (Figure 11). Benthic/planktic ratios after 7.5 Ma are in general highest at the shallowest Site 1086. At Site 1085, however, values are higher than at Site 1087 despite being about 240 m deeper.

[25] Concentrations of fish debris at Site 1085 increase from 14 Ma to peak between 11.5–10 Ma, then decrease rapidly until 9 Ma, and finally decrease gradually to 3 Ma (Figure 12). Site 1087 shows a similar pattern but with lower values, and the abbreviated record at Site 1086 also hints of a similar pattern.

[26] Terrigenous matter (mainly quartz, mica, some feldspar and rock debris) exists in very small amounts in the 63–125 μm fraction but becomes significant in the 40–63 μm fraction (Figure 13). At Site 1087, values are in general <2%. At the shallowest Site 1086, strong fluctuations between 0 and 13% occur. At Site 1085, which is nearest the Oranje River fan, three distinct terrigenous maxima of up to 20% are present between 11.5 and 9 Ma. These maxima correspond to minima in $CaCO_3$ concentrations and maxima in fish debris (Figures 5 and 12). Several spikes in terrigenous input appear between 5.5–3 Ma at Site 1085.

[27] Glauconite is rare or absent in the >63 μm fractions, whereas it is present in widely fluctuating concentrations in the 40–63 μm fraction from 6–3 Ma at the three sites (Figure 14). Prior to 9 Ma, a few percent glauconite is present at times when terrigenous matter is most abundant at Site 1085 (Figure 13). Other shelf-derived particles (thick-walled molluscs, decapods, bryozoans, relict shell material, phosphorite grains) have maxima (Figure 15) correlating with maxima in glauconite (Figure 14) and terrigenous matter (Figure 13).

[28] The proportion of pyrite crystals in the sand fraction at Site 1085 approaches 50% between 11 and 7.5 Ma (Figure 16). No pyrite is found before 12.5 Ma, and values steadily decrease after 7.5 Ma. Pyrite concentrations are much lower at Site 1087, but spikes of up to 20% between 9.2–8.5 Ma coincide with the Site 1085 pyrite peak. Pyrite is rare or absent at Site 1086 except between 7.5–7 Ma.

4. Discussion

[29] Virtually all of the descriptions of the middle-late Miocene carbonate crash and early Pliocene biogenic bloom

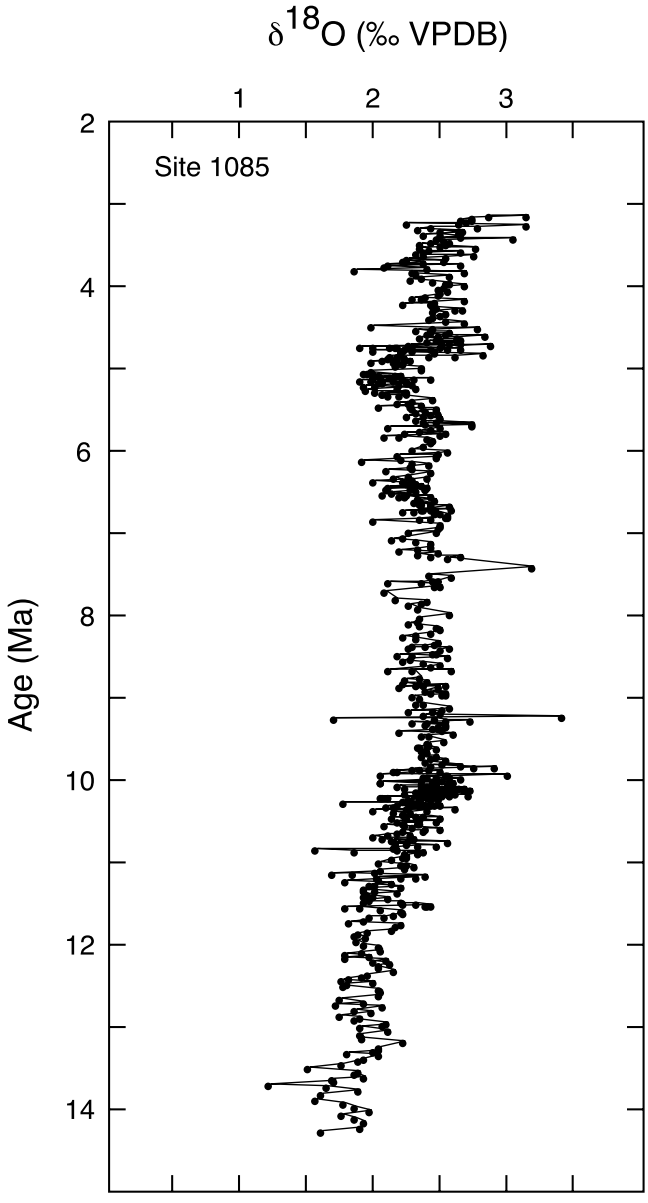

Figure 4. Benthic foram oxygen isotope curve ($\delta^{18}O$ in ‰ VPDB) for ODP Site 1085 (Westerhold and Bickert, submitted manuscript, 2003).

events are from equatorial regions of the oceans, and the causes for these impressive changes in the marine realm are still obscure. Our study in the Cape Basin, which is in the subtropical South Atlantic Ocean, provides new information about these events that helps to shed light on their possible causes. We discuss the results of our proxy measurements first in terms of the paleoprocesses that participated in the carbonate crash and then of those that led to the biogenic bloom.

4.1. Carbonate Crash Period

[30] $CaCO_3$ concentrations at Sites 1085 and 1087 show several decreases between 14 and 9 Ma (Figure 5). The deepest drop is between 9.5 and 9 Ma and is simultaneous with the "nadir" of the carbonate crash in the equatorial

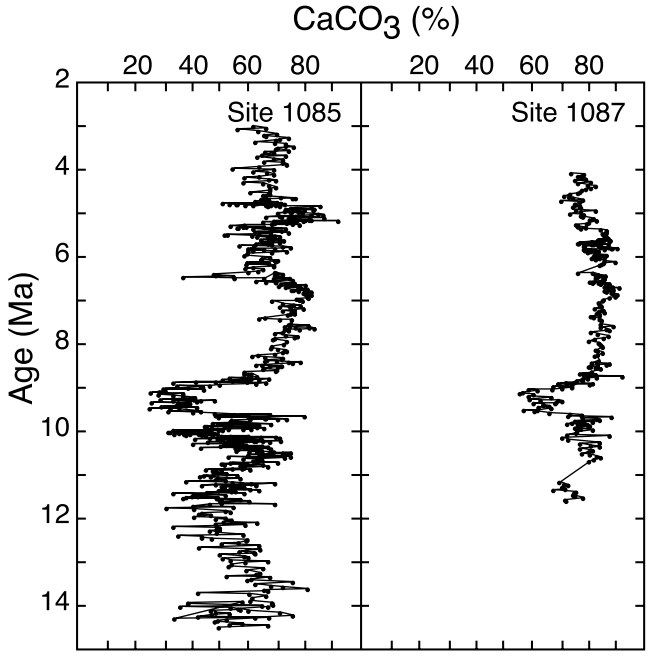

Figure 5. Concentrations of $CaCO_3$ in sediments at ODP Sites 1085 and 1087.

east Pacific Ocean [*Lyle et al.*, 1995], whereas the five carbonate minima in the Caribbean are earlier - between 12 to 10 Ma [*Roth et al.*, 2000]. These lows in $CaCO_3$ concentrations and accumulation rates are interpreted as recording times of greater carbonate dissolution as a consequence of changes in deep water circulation [*Roth et al.*, 2000].

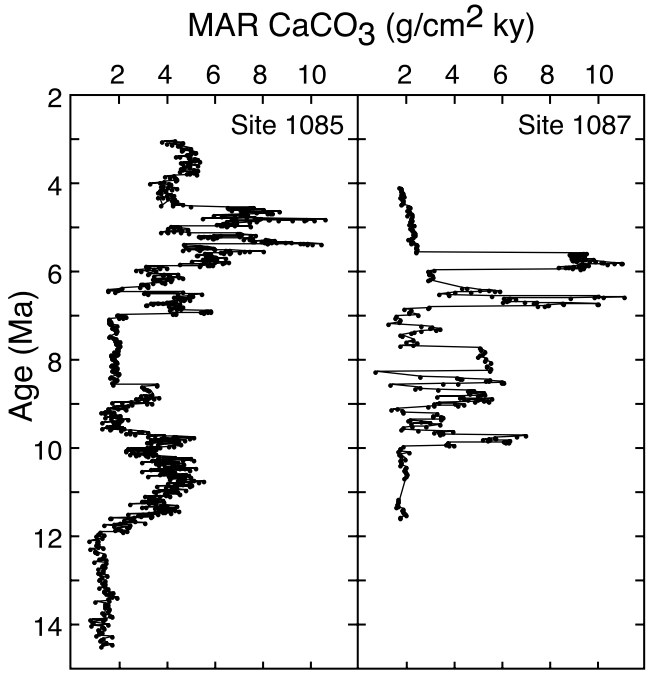

Figure 6. Mass accumulation rates of $CaCO_3$ in sediments at ODP Sites 1085 and 1087.

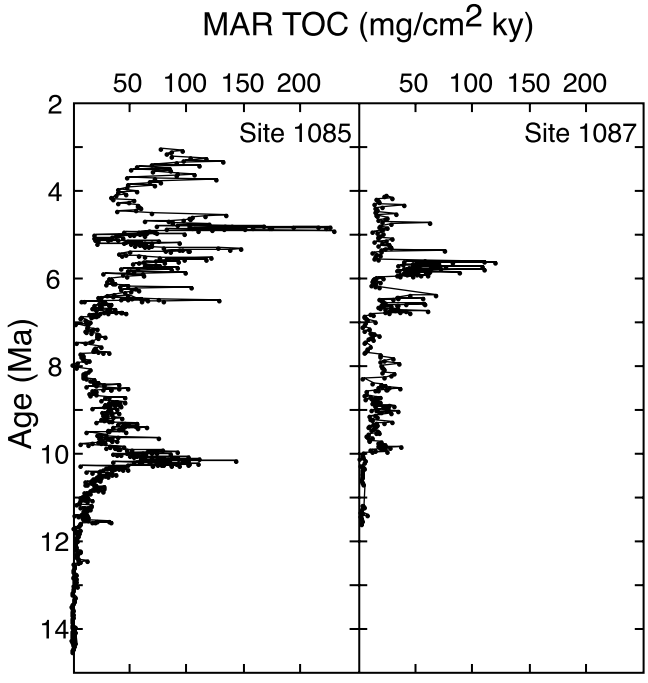

Figure 7. Mass accumulation rates of total organic carbon (TOC) at ODP Sites 1085 and 1087.

4.1.1. Evidence of $CaCO_3$ Dissolution

[31] Increases in $CaCO_3$ dissolution that left a mark on carbonate accumulation patterns should produce increases in the B/P foraminifera ratios. However, changes in the ratios (Figure 11) are not related to variations in $CaCO_3$ concentration (Figure 5). If the major depressions in $CaCO_3$ content between 12 and 9 Ma were due to carbonate dissolution, we would expect corresponding maxima in B/P ratios. However, we find B/P maxima later, after $CaCO_3$ concentrations had already recovered and terrigenous matter supply had dropped. These results reveal a decoupling of $CaCO_3$ content and carbonate dissolution as reflected in B/P ratios. We conclude that B/P ratios do not reflect only carbonate dissolution. The observation of B/P ratios that start to increase in parallel with TOC MARs (Figure 7) from 12 to 9 Ma implies that the B/P ratio is partly controlled by respiratory calcite dissolution of planktic foraminifers with increasing productivity. However, the depressions and peaks in $CaCO_3$ content do not correlate with B/P ratio variations. We therefore conclude that dissolution is not the controlling factor in the $CaCO_3$ decreases on the southwest Africa margin that correspond in time to the global carbonate crash.

4.1.2. Increases in Terrigenous Delivery and $CaCO_3$ Dilution

[32] Magnetic susceptibility values of Site 1085 sediments increase during the 12 to 9 Ma period [*Wefer et al.*, 1998a] and point to increases in clastic components that can explain the very high sedimentation rates during this time (Figure 2). The concentration of terrigenous particles in the 40–63 μm fraction increases six-fold (Figure 13) during the carbonate minima between 11.5 and 9 Ma. These silt-sized clastic grains are the "coarsest tail" of total terrigenous input and suggest that sediment supply from the nearby Oranje River was enhanced considerably. At Site 1087, which is farther from the Oranje River than Site 1085, the depression in $CaCO_3$ concentration is weaker. The amount of silt-sized terrigenous matter at this site is very low (<2% of the silt fraction) and increases only slightly during the carbonate depressions. Because Site 1087 is farther from the river, terrigenous sediment components are smaller in size and less abundant.

[33] Several factors probably contributed to the considerable increase in delivery of terrigenous matter by the Oranje River to Site 1085 between 11.5 and 9 Ma. Most important is a sea level regression that shifted the river mouth closer to the shelf edge and led to channel downcutting to a new base level. Oxygen isotope values start to increase at the same time as the terrigenous matter supply increases (Figure 4). A cooling event that increased global ice volume could have lowered sea level [*Hodell et al.*, 2002]. The *Haq et al.* [1987] sea level curve shows a major regression at about 11.5 Ma. Moreover, *Betzler et al.* [2000] report a eustatic sea level lowering at the Queensland Plateau and at the Great Bahama Bank at 10.7 Ma, which is the time of the first major spike in terrigenous matter concentrations at Site 1085 and the increase in shelf-derived particles. At Site 1085, the 11.5 Ma horizon is marked by very high content of shelf-derived particles (28% of the sand fraction), which suggests a major regression and related erosion of the shelf. Terrace development in the Namib Desert also points to a lowered sea level [*Pickford and Senut*, 1999].

[34] A sharp decrease in kaolinite and a relative increase in smectite during the 9.5 to 9 Ma major drop in $CaCO_3$ concentration are observed at Site 362 on the Walvis Ridge [*Robert and Chamley*, 1987; *Paturel*, 2000] and indicate a change to a less humid climate during this period of cooling. A shift to drier climate is also supported by an increase in proportion of grass pollen in sediments of Site 1085 after the carbonate crash [*Oboh-Ikuenobe*, 2001], as well as the onset of the fynbos succulent vegetation in the late Miocene [*Pickford and Senut*, 1999] that succeeded the middle Miocene wooded-grassland environments north of the Oranje River [*Siesser*, 1978]. With increasing aridity, the vegetative cover is likely to have become sparser and the Oranje River could have more easily eroded the land surface in its vast catchment area. The decrease in silt-sized terrigenous input and recovery of carbonate values about 2.5 My after the onset of the carbonate crash can be attributed to the late Miocene sea level highstand evidenced by fossiliferous sediments in the coastal Namib Desert [*Pickford and Senut*, 1999] and to the likelihood that loose material on the vegetation-free land surfaces had been largely eroded by this time.

[35] At 9 Ma, coarse-sized terrigenous input suddenly dropped to 1/3 to 1/4 of its former values. $CaCO_3$ concentrations sharply increase and indicate the end of the crash event, but they reach a maximum only at 7 Ma, when terrigenous input is at a minimum. Decreases in clastic supply after 9 Ma are expressed as a decrease in the >40 μm fraction (Figure 13). Reasons for these changes include rising sea level, changing climate, and reduced fluvial

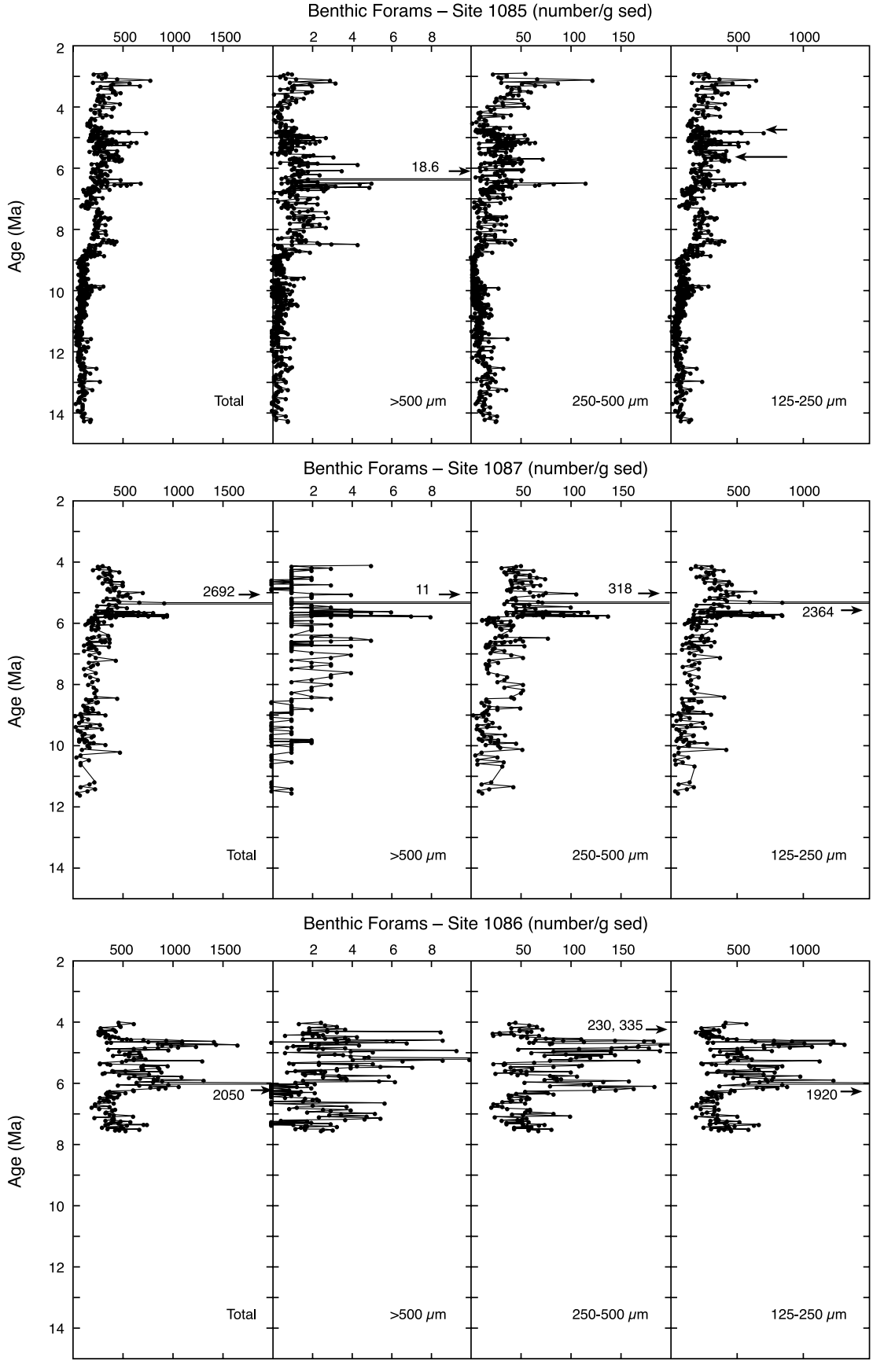
Benthic Forams – Site 1085 (number/g sed)
Age (Ma)
Total
>500 μm
250-500 μm
125-250 μm
18.6
Benthic Forams – Site 1087 (number/g sed)
2692
11
318
2364
Benthic Forams – Site 1086 (number/g sed)
2050
230, 335
1920

Figure 8.

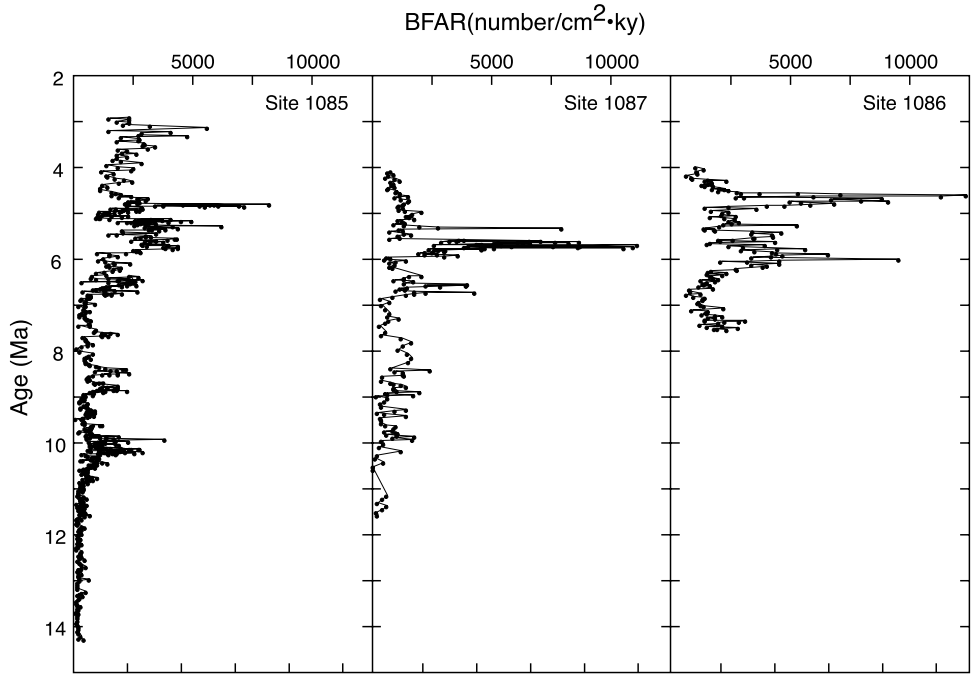

Figure 9. Benthic foraminiferal accumulation rates in numbers per cm^2 per kyr in sediments from ODP Sites 1085, 1087, and 1086.

transport. The gradual increase in $CaCO_3$ concentrations from 9 to 7 Ma underscores the importance of terrigenous input as the main factor controlling carbonate concentrations. Site 1087, which is located at greater distance from Oranje River, received less terrigenous matter in the >40 and <40 μm fractions and consequently shows a much smaller reduction in $CaCO_3$ content during the crash events. We consequently conclude that increases in terrigenous input were primarily responsible for the carbonate decreases between 12.5 and 9 Ma on this margin.

4.1.3. Paleoproductivity Changes

[36] B/P ratios are sensitive to productivity as well as to carbonate dissolution. We therefore wondered whether the gradual increase in B/P ratios from 12 to 8 Ma indicates gradually increasing export paleoproductivity. We enlisted additional paleoproductivity proxies to address this important question. Both the NBF and BFAR increased between 11 and 9.7 Ma (Figures 8 and 9), but they were lowest during the major $CaCO_3$ depression at 9.5 to 9 Ma (Figure 5). TOC MARs, another proxy for paleoproductivity, also began to increase at 11 Ma and reached a maximum between 10 to 9 Ma (Figure 7). However, at 9 to 8 Ma when B/P ratios were highest, TOC MARs, BFARs and NBF decreased. In contrast, organic matter $\delta^{13}C$ values remained about −23.5‰ from 14 to 11 Ma and then increased to fluctuate around −22.0‰ until 8 Ma [*Twichell et al.*, 2002], which suggests increased paleoproductivity from 11 to 8 Ma. Consensus between the different paleoproductivity proxies does not exist.

[37] A pattern of gradually increasing productivity from 12 to 9 Ma is supported elsewhere in the ocean by higher phosphate mass accumulation rates (PMAR) at Site 526 (western Walvis Ridge) and Site 757 (Ninety East Ridge) [*Hermoyian and Owen*, 2001]. During the same time, *Uvigerina* numbers, which are a good proxy for export productivity [*Berger et al.*, 2002], increased at these sites (L. Diester-Haass, unpublished results, 2002).

[38] A possible explanation for some of the discrepancies between the various paleoproductivity proxies may be found in the variations in fish debris and pyrite in our sediments. The amounts of fish debris, rare before 12.5 and after 8 Ma, increase and decrease parallel with terrigenous input between 12.5 and 9 Ma (Figures 12 and 13). Pyrite appears for the first time at 12.5 Ma with the first spike in terrigenous input and increases gradually until reaching a maximum between 9.5 and 8.5 Ma that occurs shortly after the spikes in terrigenous input (Figure 16). Three factors control pyrite formation: abundance of (1) TOC, (2) reactive detrital Fe, and (3) dissolved sulfate [*Emeis et al.*, 1991]. The onset of increased terrigenous sediment delivery at about 12.5 Ma probably increased detrital Fe availability [*Wefer et al.*, 1998b]. Increasing productivity led to higher TOC MARs (Figure 7). Greater sedimentation of organic matter enhanced oxygen depletion in the uppermost sedi-

Figure 8. Number of benthic foraminifers >125 μm in 1 g of sediment found in sediments from ODP Sites 1085, 1087, and 1086 and their size distribution, expressed as numbers of foraminifers sized 125–250 μm, 250–500 μm, and >500 μm in 1 g of sediment. Arrows at Site 1085 highlight intervals discussed in text where numbers of smaller foraminifers increase and coarser ones decrease.

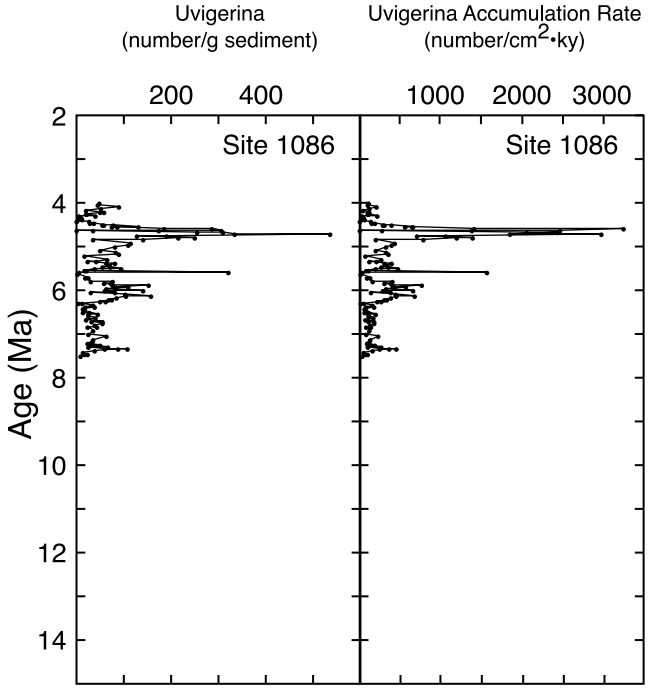

Figure 10. Concentrations and accumulation rates of the benthic foram genus *Uvigerina* in sediments from ODP Site 1086.

ment layers, reduced interstitial sulfate, and increased pyrite formation. Oxygen depletion was probably greatest 9.8 to 9 Ma where pyrite content is highest (Figure 16). These oxygen-depleted sediments were hostile to benthic fauna; we find lowest NBF and BFAR from 9.8 to 9 Ma despite the high paleoproductivity indicated by TOC MARs. Preservation of fish debris, whose apatite and cartilaginous skeletal material is rapidly dissolved in well-oxygenated environments, is improved under these circumstances. After 6.7 Ma fish debris is rare despite high productivity because of good oxygenation of bottom and pore waters. These considerations lead us to conclude that regional paleoproductivity was elevated from 12 to 9 Ma.

4.1.4. Water Mass Changes

[39] From 12.5 to 9 Ma, carbonate dissolution varies in parallel with pyrite, productivity proxies, and terrigenous input. We expected to find a drop in carbonate dissolution simultaneous with the sharp reduction in coarse terrigenous supply at 9 Ma. Instead, carbonate dissolution increases (Figure 13) after the 9.5 to 9 Ma crash event until reaching maxima of up to 50% B/P between 8.5 and 7.5 Ma. Other processes are evidently involved, inasmuch as terrigenous matter, productivity proxies and pyrite content decrease when carbonate dissolution (B/P ratio) is at its maximum. We attribute this finding to a change in ocean circulation and bottom water masses.

[40] Site 1085 is presently within the upper part of the North Atlantic Deep Water (NADW) [*Siedler et al.*, 1996], which is a well oxygenated and carbonate-ion-rich water mass that preserves $CaCO_3$ well [*Gerhardt and Henrich*, 2001; A. N. A. Volbers and R. Henrich, unpublished manuscript, 2003, hereinafter referred to as Volbers and Henrich, unpublished manuscript, 2003]. The overlying Upper Circumpolar Deep Water (UCDW) is at a depth between 900 and 1400 m and is not as well oxygenated and has lower carbonate ion concentrations. Sediments deposited within this water mass show stronger carbonate

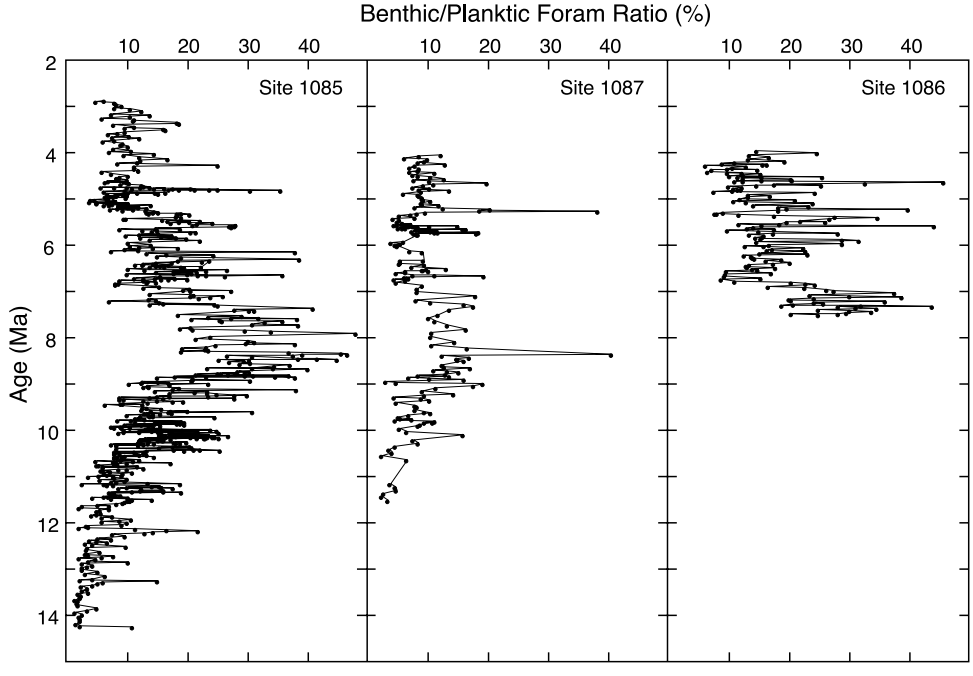

Figure 11. Benthic/planktic foraminiferal ratio, expressed as the percent of benthic forams in the total of benthic plus planktic forams, in sediments from ODP Sites 1085, 1087, and 1086.

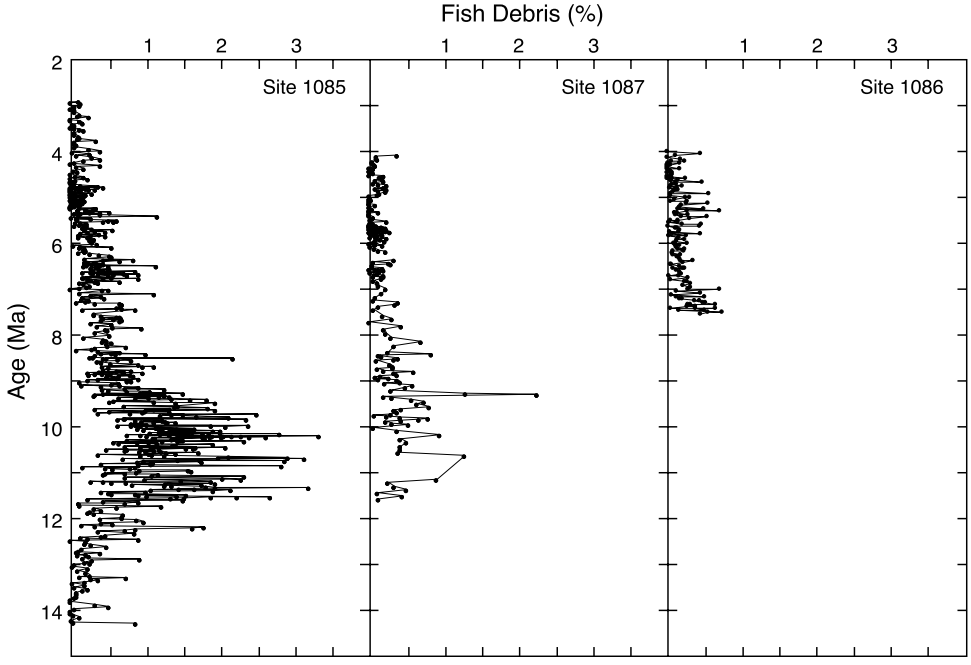

Figure 12. Concentrations of fish debris in the sand fraction (>63 μm) of sediments from ODP Sites 1085, 1087, and 1086.

dissolution (Volbers and Henrich, unpublished manuscript, 2003). Antarctic intermediate water presently lies between 400 and 900 m and probably did not influence Miocene-Pliocene sediments at the depth of ODP Site 1085.

[41] Information on the Miocene paleohydrography in the southeast Atlantic is sparse. *Woodruff and Savin* [1989] believe that from 10 to 6 Ma the thermohaline circulation in the Atlantic resembled modern circulation in many ways. The existence of a NADW is assumed since the late Miocene - about 10 Ma by many authors [*Woodruff and Savin*, 1989; *Wright et al.*, 1991; *Hay and Brock*, 1992; *Farrell et al.*, 1995; *Berger and Wefer*, 1996; *King et al.*,

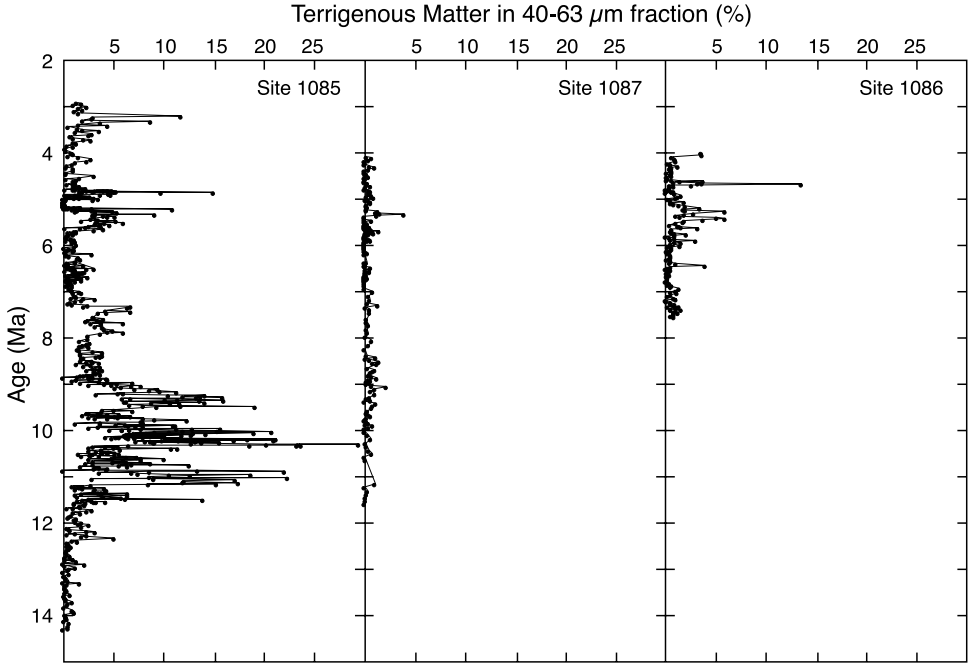

Figure 13. Contributions of terrigenous material (%) to the total 40–63 μm fraction of sediments from ODP Sites 1085, 1087, and 1086.

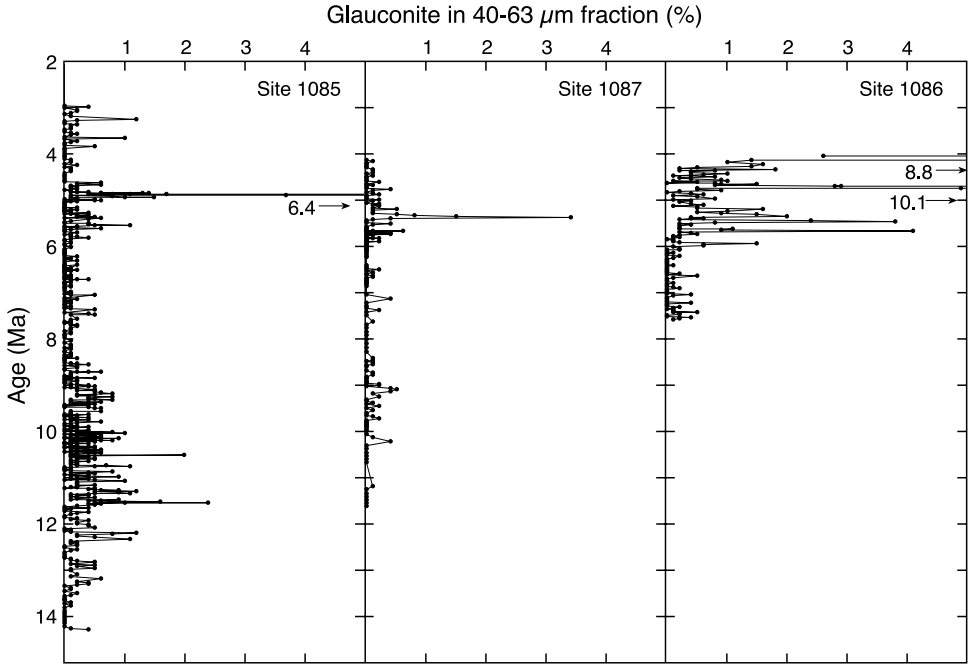

Figure 14. Concentration of glauconite in the 40–63 μm fraction of sediments from ODP Sites 1085, 1087, and 1086.

1997] and even a few million years earlier by others [*Ramsay et al.*, 1998; *Frank et al.*, 2002]. The NADW was overlain by a southern component water above about 1200 m depth at 30°S in the late Miocene [*Frank et al.*, 2002]. If the physicochemical properties of these late Miocene water masses were comparable to present-day ones, our finding of increased $CaCO_3$ dissolution might be due to deepening of the UCDW-NADW boundary. During the 9 to 7 Ma period, when unusually strong carbonate dissolution cannot be related to productivity and

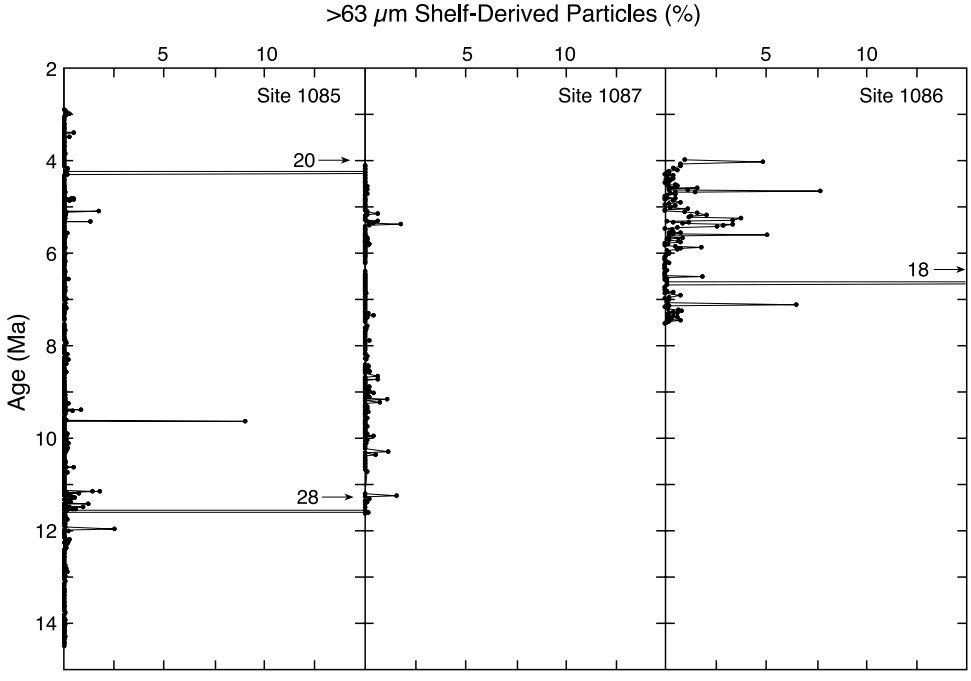

Figure 15. Concentration shelf-derived particles (coarse mollusc debris, relict shell material, decapods, bryozoans, phosphorite) in the sand fraction (>63 μm) of sediments from ODP Sites 1085, 1087, and 1086.

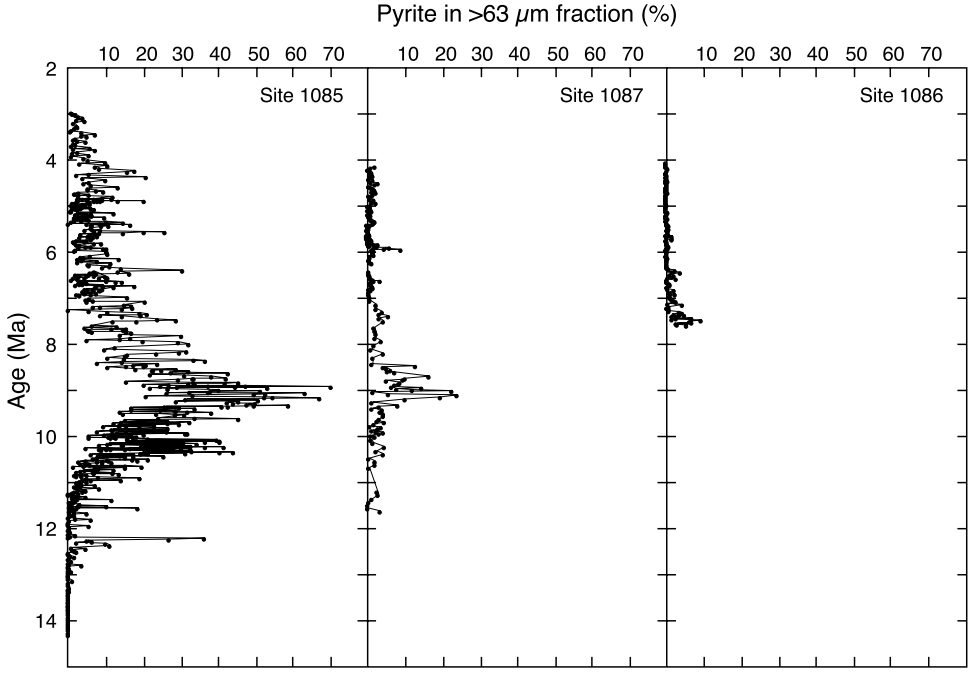

Figure 16. Concentration of pyrite in the sand fraction (>63 μm) of sediments from ODP Sites 1085, 1087, and 1086.

metabolic CO_2 generation, we propose the presence of an oxygen-poor UCDW that led to stronger dissolution of planktic foraminifers. This proposal is supported by findings of *Diekmann et al.* [2003], who attribute carbonate depleted sediments at 8 Ma from ODP Site 1088 on the Agulhas Ridge to a strong influence of corrosive circumpolar deep water (CPDW). The initiation of Northern Hemisphere glaciation at 7 Ma [*Larsen et al.*, 1994] probably strengthened the flow of NADW [*Berger and Wefer*, 1996; *King et al.*, 1997] and raised the UCDW-NADW boundary such that Site 1085 was within NADW. Such a change in water mass is supported by benthic foraminiferal $\delta^{13}C$ values from Site 1088 that show an increase in northern component water masses at 6.6 Ma and larger than present-day amounts in the early Pliocene [*Billups*, 2002]. This finding can explain why carbonate dissolution has been weaker since 6.7 Ma, although strongly fluctuating, despite highly increased paleoproductivity. Pyrite content dropped after this hydrographic change because of good oxygenation in bottom and pore waters.

4.1.5. Cause of the Carbonate Crash on the Southwest Africa Margin

[42] We conclude that the three major depressions in carbonate concentrations between 12 and 9 Ma were caused by strong terrigenous dilution of biogenic carbonate. The influence of productivity on the carbonate concentration depressions is less clear. Export productivity increased from 12–10 Ma, as can be seen in the increase in BFAR. The increase in $CaCO_3$ MAR since 12 Ma points to enhanced production of calcareous nannoplankton. We cannot determine whether the elevated productivity is related to the first appearance of upwelling influence or to enhanced fluvial nutrient input; either could have caused the gradual increases in $CaCO_3$ MAR, TOC MAR, BFAR, and NBF. However, it is clear that during the time of the strongest decrease in carbonate concentration and highest pyrite content at 9.5 to 9 Ma, productivity was lower than prior to 10–9.5 Ma, as can be seen in lower $CaCO_3$ MAR and TOC MAR. Bottom water oxygen depletion was such that benthic life suffered and NBF and BFAR decreased.

4.1.6. Paleoceanographic Implications

[43] During the middle-to-late Miocene, strong decreases in carbonate concentrations occurred in equatorial regions of all major oceans and have been attributed to dissolution as a consequence of the rise in the CCD [*Van Andel and Health*, 1975]. In the Caribbean, five major dissolution spikes between 12 and 10 Ma correspond to pulses of NADW [*Roth et al.*, 2000]. In the eastern equatorial Pacific, the carbonate crashes are dissolution events related to low productivity between 12 and 9 Ma that have been attributed to tectonic restriction of deep water flow through the Panama gateway [*Lyle et al.*, 1995; *Farrell et al.*, 1995]. At locations in the equatorial Atlantic Ocean, on the Ceara Rise [*Shipboard Scientific Party*, 1995], in the South Atlantic [*Hsü and Wright*, 1985], on the Ontong Java Plateau [*Berger et al.*, 1993], and in the Indian Ocean [*Petersen et al.*, 1992], the interval of low carbonate accumulation extends from 9 Ma back until the middle or even early Miocene and has been attributed to a rise in the CCD and low paleoproductivity [*Peterson et al.*, 1992]. A correlation between low $CaCO_3$ accumulation rate and high sea level during the middle Miocene suggests repartitioning of carbonate to the shelves instead of the deep seafloor [*Berger et al.*, 1993]. However, *Lyle et al.* [1995] argue that the Miocene transgressions were interrupted by the middle-late Miocene regression, which should have increased deep-

sea $CaCO_3$ concentrations and lowered the CCD. In the absence of these changes, they rule out sea level change as a major factor in causing the carbonate crash.

[44] Our results conflict with others in showing that dilution of carbonates by terrigenous matter during the carbonate crash interval is responsible for the low carbonate concentrations off southwest Africa. Furthermore, local productivity increased during the crash events, contrary to interpretations of *Lyle et al.* [1995]. Our results are the first from a subtropical continental margin, and they are from relatively shallow water depths of 1800 to 1300 m. Thus they probably reflect local processes, such as increased flow of the nearby Oranje River, in addition to global phenomena.

[45] A broader aspect of the changes in clastic sedimentation that are evidently important on the southwest Africa margin emerges from the estimates of average global Cenozoic sedimentation rates produced by *Davies et al.* [1977]. A synchronous increase in carbonate and total sedimentation rates in the late Miocene (11.2–5.2 Ma, recalculated to *Berggren et al.* [1995] ages) in the three major ocean basins points to a global increase in weathering and dissolved nutrient supply to the oceans. Similarly, *Rea* [1992] calculates a five-fold increase in terrigenous flux to the northern Indian Ocean at about 12.6 Ma (recalculated to *Berggren et al.* [1995] ages) as a result of the Himalaya uplift. These aspects imply that not only lowered sea level but also a global change in atmospheric circulation might have led to the locally increased weathering and erosion that yielded the increased terrigenous input to the southwest Africa margin during the time of the carbonate crash.

4.2. Biogenic Bloom Period

4.2.1. Evidence of Paleoproductivity Changes on the Southwest Africa Margin

[46] Paleoproductivity, as reflected in NBF, BFAR, and TOC MAR, gradually increases after 12.5 Ma at Sites 1085 and 1087. Between 7 to 6 Ma, however, a major change to higher and more widely fluctuating paleoproductivity proxy values occurred. The paleoproductivity fluctuations covary with changes in LSRs (Figure 2). Unlike the 11.5 to 9.5 Ma period when the high LSRs are related to a strong increase in terrigenous input, the terrigenous matter concentrations are low and $CaCO_3$ contents are high. A similar increase in mass accumulation rates of biogenic carbonate has also been observed on the Walvis Ridge at this time [*Siesser*, 1980; *Cepek et al.*, 1999].

[47] The increase in LSR is most likely a consequence of increasing paleoproductivity. Further support for increasing productivity since 6.7 Ma comes from Site 1086 where *Uvigerina spp.* numbers and accumulation rates, both tested tracers of high export productivity [*Berger al.*, 2002], increase in parallel with BFAR and NBF (Figures 8, 9, and 10). In addition, organic matter $\delta^{13}C$ values at Site 1085 increase from −23.0‰ to −21.5‰ at about 6.5 Ma [*Twichell at al.*, 2002], which is yet more evidence of a productivity increase at this time.

[48] The concentration of sand fraction and the MAR of carbonate increase parallel to the increase in paleoproductivity proxies at about 6.7 Ma (Figures 3 and 5). It is interesting to note that at Site 926 on the Ceara Rise of the equatorial Atlantic Ocean, fluxes of the sand fraction [*Shackleton and Crowhurst*, 1997] and $CaCO_3$ [*Murray and Petersen*, 1997] show the same pattern, which has been attributed to an increase in "blue ocean productivity" and to a decrease in carbonate dissolution after 6.5 Ma [*Shackleton and Crowhurst*, 1997]. Our results support this interpretation; the increase in our sand fraction concentrations parallels a decrease in carbonate dissolution. This agreement points to a possible Atlantic-wide oceanographic change since 6.5 Ma, related perhaps to an intensification and extension of NADW flow. Furthermore, we observe an increase in paleoproductivity that is not accompanied by an increase in $CaCO_3$ dissolution, as also seen by *Murray and Petersen* [1997] on the Ceara Rise. Dissolution often increases with increased delivery of organic matter [*Archer and Meier-Reimer*, 1994].

[49] The onset of high paleoproductivity at 6.7 Ma is not related to a significant change in $\delta^{18}O$ values (Figure 4). However, *Kennett* [1995] describe a major regression related to the expansion of Antarctic ice shelves at 6.5 to 5 Ma, and three of our major increases in productivity after 6.7 Ma are related to heavy $\delta^{18}O$ values (5.8 to 5.4, 4.9 to 4.6, and 3.3 to 3.1 Ma). If these $\delta^{18}O$ maxima are due to global cooling and ice growth, sea level should have been lowered. *Haq et al.* [1987], *Aharon et al.* [1993], and *Vidal et al.* [2002] assume about a 40 m drop in sea level in the late Miocene. In fact, evidence for lowered sea level exists at Site 1085 in the form of an increase in glauconite (Figure 14), which comes from the shelf [*Rogers and Bremner*, 1991] and is more easily transported downslope during regressions. At the shallowest site (1086), glauconite percentages are highest, and shallow-water particles such as thick-walled or worn mollusc shells and phosphorite grains indicate downslope transport processes, as do terrigenous matter concentrations that parallel glauconite abundances. However, Site 1087, which is about 500 m deeper than Site 1086, contains no hint of sediment supply from shallow water during the 4.9 to 4.6 Ma cool period when a major regression is likely.

[50] We cannot completely exclude that benthic foraminifers have also been transported downslope from shallow water, as small sized foraminifers (125–250 μm) increase in two intervals at Site 1085 compared to the larger ones that decrease (Figure 11) [*Diester-Haass et al.*, 2002]. However, at Sites 1086 and 1087, the 250–500 and >500 μm sized foraminifers increase in parallel to the small ones (Figure 8). As neither glauconite nor other shallow water particles are found in fractions >250 μm, we assume that benthic foraminifers >250 μm are autochthonous. If large foraminifers increase in parallel to small ones, it can be assumed that this is due to production and not to lateral supply of small foraminifers.

[51] If only water depth controls the NBF and BFAR values and TOC MARs, we should expect a progressive decrease from Site 1086 to Site 1087 to Site 1085. This change should exist because the organic matter supply, and thus food for benthic organisms, decreases with depth if there is not an additional source of organic particles, such as near-bottom downslope transport of suspended organic

matter from the outer shelf [*Diester-Haass et al.*, 1992; *Sancetta et al.*, 1992; *Summerhayes et al.*, 1995]. Our results show that such an additional source must have been active, because BFAR and TOC MAR values are in general highest at the deepest Site 1085, except for the 5.8 to 5.6 Ma interval, where BFAR values increase at Site 1087. B/P values, which normally decrease with increasing water depth [*Berger and Diester-Haass*, 1988], correlate to that finding by being higher at Site 1085 than at the shallower Site 1087. We argue that Site 1085 received a greater food supply and thus shows higher BFAR and B/P ratios than the shallower sites. The terrigenous input from the Oranje River must be considered as a potential additional source of food, either by fertilizing surface waters with dissolved nutrients or by adsorption of organic matter on clay mineral surfaces. Higher glauconite contents at Site 1085 compared to the shallower Site 1087 underscore the increased influence of downslope transport processes (Figure 14) on the continental slope, which is steeper in the region of Site 1085 compared to the two more southerly locations.

[52] We conclude that primary productivity increased considerably and fluctuated strongly off southwest Africa after about 6.7 Ma. Increased organic matter supply from the photic zone raised TOC contents of the sediments and enhanced benthic foraminiferal production rates. Some of these paleoproductivity maxima occurred in cooler periods (Figure 4), when sea level was likely to have been lowered. Downslope transport of originally shallower sediment components may have amplified the paleoproductivity signals of BFAR and TOC MAR at these times.

4.2.2. Origins of Paleoproductivity Increase on Southwest Africa Margin

[53] The paleoproductivity increase we find may reflect the onset of regional upwelling [*Summerhayes et al.*, 1995], or it could be part of a global change in oceanic productivity. If upwelling processes influenced the signal of high paleoproductivity at our sites beyond the shelf edge, westward flowing filaments of upwelled water would need to transport nutrients to our sites and thus enhance benthic foraminiferal production and increase TOC MARs. In this case, we would expect to find a decrease in paleoproductivity signals with increasing distance from the shelf edge. Site 1085 presently lies within a center of such a filament of upwelled water [*Wefer et al.*, 1998a] and has higher productivity events than the southern locations. However, as we cannot separate the influence of river fertilization from possible upwelling effects, this finding does not allow any conclusion as to upwelling history. Comparing Sites 1086 and 1087 does not allow conclusions as to possible upwelling either, because the higher BFAR at Site 1086 can be explained by shallower water depth alone.

[54] The question of when the onset of upwelling occurred cannot be answered from biogenic opal, although it is a significant component of Pliocene and Quaternary sediments on the Walvis Ridge [*Diester-Haass et al.*, 1990, 1992; *Sancetta et al.*, 1992; *Lange et al.*, 1999; *Anderson et al.*, 2001; *Berger et al.*, 1998, 2002]. No opal is found in the Miocene sequences at Sites 1086 and 1087. At Site 1085, minor amounts at 5.8 and 5.2 Ma record the southernmost extension of silica-enriched intermediate water [*Diester-Haass et al.*, 2002; *Anderson et al.*, 2001]. *Lange et al.* [1999] and *Marlow et al.* [2000] observe that late Miocene and early Pliocene diatoms from Site 1082 on the Walvis Ridge and Site 1084 in the northern Walvis Basin are oligotrophic warm-water species. These findings imply that local upwelling processes, which supply cool water and related upwelling-specific assemblages, are not solely responsible for the late Miocene increases in paleoproductivity in the Cape Basin that correspond to the global biogenic bloom.

[55] Examination of late Miocene records from other widespread locations suggests that the productivity history in the Cape Basin is instead linked to global productivity variations. Increases in LSR and productivity similar to those at Site 1085 appear at locations in the equatorial Pacific Ocean [*Van Andel and Health*, 1975; *Berger et al.*, 1993; *Farrell et al.*, 1995], the equatorial Indian Ocean [*Peterson et al.*, 1992; *Dickens and Owen*, 1999], the northwest Pacific Ocean [*Rea et al.*, 1995], the southwest Pacific Ocean [*Grant and Dickens*, 2002], and the subpolar South Atlantic Ocean [*Froelich et al.*, 1991; *Diekmann et al.*, 2003]. For example, in the equatorial Pacific Ocean LSRs increase by a factor of 5 and more between 7 and 6 Ma. These increases in LSRs correspond to dramatic increases in productivity proxies such as MARs of opal, carbonate, phosphorus, and barium [e.g., *van Andel and Health*, 1975; *Schroeder et al.*, 1997]. Furthermore, the equatorial Pacific locations as well as Site 704 on the Meteor Rise [South Atlantic] show the same well-developed temporal variability in productivity during the high productivity interval as does Site 1085 [*Schroeder et al.*, 1997; *Farrell et al.*, 1995; *Froelich et al.*, 1991]. According to the best available chronostratigraphy, the shift at Site 1085 began at 6.7 to 6.5 Ma, and the time given by *Farrell et al.* [1995] for the onset of the biogenic bloom in the equatorial east Pacific is 6.7 Ma (their timescale is based on *Shackleton et al.* [1995], which for the 7 to 6 Ma period corresponds to *Berggren et al.* [1995]). The shift to higher productivity at the subpolar location Site 704 is at 6.9 Ma [*Froelich et al.*, 1991], after adjusting to the timescale of *Berggren et al.* [1995], and at 6.5 Ma at ODP Sites 1088 and 1092 [*Diekmann et al.*, 2003].

4.2.3. Paleoceanographic Implications

[56] The productivity increase in the latest Miocene (6.9 to 6.5 Ma) at widespread locations raises several questions: (1) Was the increase a consequence of redistribution of nutrients within the oceans?, (2) Was it a response to an increase in supply of nutrients to the oceans?, and (3) Are the carbonate crash and the biogenic bloom events related?

[57] Two mechanisms that could have redistributed nutrients within ocean basins are gradual shoaling of the Isthmus of Panama [*Farrell et al.*, 1995, and references therein] and onset of NADW formation [*Berger et al*., 1995; *Wright et al.*, 1991]. However, *Farrell et al.* [1995] did not find a temporal link between the history of NADW and the onset of the biogenic bloom. Potential effects of the Messinian salinity crisis [*Hodell et al.*, 1994] are too late according to the revised dating (6.0–5.3 Ma) by *Krijgsman et al.* [1999] to have initiated the biogenic bloom.

[58] This period of the late Miocene biogenic bloom is characterized by sediment hiatuses at most southern high-latitude locations [*Barker et al.*, 1990; *Barron et al.*, 1991; *Wise et al.*, 1992; *Exon et al.*, 2001]. Nonsedimentation in the Southern Ocean and major increases in biogenic production and sedimentation at low latitudes point to a redistribution of nutrients within ocean basins. The growth of the west Antarctic ice sheets [*Shackleton and Kennett*, 1975; *Kennett*, 1995; *Hodell et al.*, 1994, 2002 and references therein] and initiation of Northern Hemisphere ice caps at 7 Ma [*Larsen et al.*, 1994] may have affected vertical nutrient distribution by increasing the equator-to-pole temperature gradient and thus intensifying atmospheric and oceanic zonal circulation and therefore mixing in the ocean. A similar mechanism is also probably responsible for the sudden rise in marine biological productivity in the earliest Oligocene during the substantial growth of Antarctic ice sheets [*Diester-Haass and Zahn*, 1996, 2001].

[59] Another candidate to explain the latest Miocene biogenic bloom is enhanced flux of dissolved nutrients to the oceans [*Dickens and Owen*, 1999]. The onset of Indian Ocean monsoons at 7 to 6 Ma. [*Molnar et al.*, 1993], a time that has been supported by climate modeling [*Prell and Kutzbach*, 1992], may have increased chemical weathering of the continents and enhanced fluvial fluxes to the oceans. Increased delivery of Ca and Si and other nutrients necessary for the increased production of carbonate and opaline fossils that is observed in the latest Miocene may have been the consequence. A possible effect of monsoon circulation on wind systems in other parts of the world could be expected. Southeast trade winds may have intensified and contributed to the productivity increase between 6.7 to 6.5 Ma at Site 1085.

[60] Our evidence of an export productivity increase at 6.7 to 6.5 Ma in the Cape Basin does not permit us to distinguish unequivocally between a local change in upwelling processes and thus onset of upwelling circulation off southwest Africa or to global changes in nutrient distribution or supply. We also cannot rule out a geochemical link between the middle/late Miocene carbonate crash as observed in the Caribbean [*Roth et al.*, 2000], the equatorial Pacific [*Lyle et al.*, 1995; *Berger et al.*, 1993] and the South Atlantic [*Berger and Wefer*, 1996], that ended about 2 My before the onset of high productivity. However, the coincident timing of similar increases in productivity at the many distant locations is striking, and it suggests the existence of a global connection of some kind.

5. Conclusions

[61] Middle-late Miocene to early Pliocene sediments from the southwest African continental margin provide new information about the carbonate crash and biogenic bloom events that have previously been described from the equatorial regions of the ocean basins. The principal cause of the carbonate crash off southwest Africa, evident as several sharp drops in $CaCO_3$ concentration between 12 and 9 Ma, is an increased delivery of clastic matter from the Oranje River. Carbonate dissolution as reflected on B/P ratios is not related to the carbonate drops. This is most evident at Site 1085, which is located close to the outer edge of the Oranje fan, and less pronounced at Site 1087, 200 km south of Site 1085. A sea level regression at the middle/late Miocene transition shifted the river mouth closer to the shelf edge and increased delivery of the river sediment load to the continental slope. The role of terrigenous dilution as the main agent in creating the drops in $CaCO_3$ during the 12 to 9 Ma period along the southwest Africa margin contrasts with the origin of the carbonate crash events in offshore areas of the equatorial Indian and Pacific Oceans, which were caused by carbonate dissolution [*Peterson et al.*, 1992; *Lyle et al.*, 1995; *Berger et al.*, 1993].

[62] Paleoproductivity, as reflected by TOC MAR, NBF and BFAR, began to increase at 12 Ma, coincident with the increase in terrigenous input. We cannot determine whether the onset of early upwelling or fertilization by dissolved river load is responsible. During the nadir of the carbonate crash at 9.5 to 9.0 Ma, when $CaCO_3$ was at its minimum and TOC was elevated, the NBF and BFAR paleoproductivity proxies have low values because oxygen depletion restricted benthic life. High amounts of fish debris and pyrite crystals record productivity-driven decreases in bottom oxygenation between 12 and 9 Ma.

[63] At 9 Ma, carbonate values recovered and gradually increased to a maximum at 7 Ma in response to a gradual decrease in terrigenous input as indicated by decreasing magnetic susceptibility of sediments. Carbonate dissolution, however, does not correlate to the increasing $CaCO_3$ concentrations, as it has a maximum during the time of recovery of $CaCO_3$ concentrations between 8.5 and 7.5 Ma. We believe that different processes control carbonate dissolution before and after 9 Ma. Between 12–9 Ma, carbonate dissolution can be attributed to changes in paleoproductivity and related benthic bacterial activity, plus lowered oxygenation of bottom and pore water in the rapidly deposited terrigenous muds. Since 9 Ma, however, major changes in water mass distribution are proposed for the carbonate dissolution maximum during a period of low paleoproductivity and improving oxygenation of bottom and pore waters. During the 9 to 7 Ma period, Site 1085 was likely within the Upper Circumpolar Deep Water whose low carbonate ion concentration and low oxygen content would have favored carbonate dissolution. With the onset of Northern Hemisphere glaciation at about 7 Ma [*Larsen et al.*, 1994], the North Atlantic Deep Water expanded upward to cover Site 1085 and created much better but fluctuating carbonate preservation despite higher surface productivity.

[64] At about 6.7 Ma, paleoproductivity increased off southwest Africa by factors of up to 7 to 9 and fluctuated strongly. Some of the maxima in TOC MAR, NBF, and BFAR are during cooler periods, when sea level was lower and cross-shelf transport brought glauconite and shell material to the continental slope. The onset of high paleoproductivity off southwest Africa is simultaneous with that in the eastern equatorial Pacific [*Farrell et al.*, 1995], western equatorial Pacific [*Berger et al.*, 1993] and Indian Ocean [*Peterson et al.*, 1992; *Dickens and Owen*, 1999]. We believe that the late Miocene southwest African paleoproductivity increase is related to a global increase in paleo-

productivity and not to the regionally increased paleoproductivity related to the strength of upwelling in the Benguela Current Upwelling System, which peaked at about 3 Ma [*Meyers et al.*, 1983; *Marlow et al.*, 2000].

[65] **Acknowledgments.** Discussions with W. Berger, G. Wefer, and L. Vidal were especially helpful in interpreting the analytical results. We gratefully acknowledge thoughtful comments from Larry Peterson and two anonymous reviewers. We thank the Ocean Drilling Program, funded by the National Science Foundation and IPOD countries, for providing the sediment samples. Achim Schmidt and Marco Hinsberger prepared the samples for the different analyses. Shannon Twichell and Christina Knowlton performed the carbon analyses. PAM is grateful for the unique experience of studying the evolution of the Benguela Current Upwelling System during both DSDP Leg 75 and ODP Leg 175 and to the Hanse-Wissenschaftskolleg (Delmenhorst) for providing the contemplative and creative setting in which to contribute to this document. Funding from the Deutsche Forschungsgemeinschaft and JOI-USSAC supported this study.

References

Aharon, P., S. L. Goldstein, C. W. Wheeler, and G. Jacobsen (1993), Sea-level events in the South Pacific linked with the Messinian salinity crisis, *Geology*, *21*, 771–775.

Anderson, P. A., C. D. Charles, and W. H. Berger (2001), Walvis paradox confirmed for the early Quaternary at the southern end of the Namibia upwelling system, ODP Site 1085, Ocean Drill, Program, College Station, Tex.. (Available at http://www-odp.tamu.edu/publications/175_SR/chap_21/chap_21.htm.)

Archer, D., and E. Maier-Reimer (1994), Effect of deep-sea sedimentary calcite preservation on atmospheric CO_2 concentration, *Nature*, *367*, 260–263.

Barker, P. F., et al. (1990), *Proceedings of the Ocean Drilling Program, Initial Reports*, vol. 113, 785 pp., Ocean Drill. Program, College Station, Tex.

Barron, J., et al. (1991), *Proceedings of the Ocean Drilling Program, Initial Reports*, vol. 119, 982 pp., Ocean Drill. Program, College Station, Tex.

Berger, W. H., and L. Diester-Haass (1988), Paleoproductivity: The benthic-planktonic ratio in foraminifera as a productivity index, *Mar. Geol.*, *81*, 15–25.

Berger, W. H., and G. Wefer (1996), Expeditions into the past: Paleoceanographic studies in the South Atlantic, in *The South Atlantic: Present and Past Circulation*, edited by G. Wefer et al., pp. 363–410, Springer-Verlag, New York.

Berger, W. H., R. M. Leckie, T. R. Janecek, R. Stax, and T. Takayama (1993), Neogene carbonate sedimentation on Ontong Java Plateau: Highlights and open questions, *Proc. Ocean Drill. Program Sci. Results*, *130*, 711–744.

Berger, W. H., G. Wefer, C. Richter, C. B. Lange, J. Giraudeau, and O. Hermelin (1998), Shipboard Scientific Party. The Angola-Benguela upwelling system: Paleoceanographic synthesis of shipboard results from leg 175, *Proc. Ocean Drill. Program Initial Rep.*, *175*, 505–530.

Berger, W. H., C. B. Lange, and G. Wefer (2002), Upwelling history of the Benguela-Namibia system: A synthesis of Leg 175 results, Ocean Drill, Program, College Station, Tex. (Available at http://www-odp.tamu.edu/publications/175_SR/synth/synth.htm.)

Berggren, W. A., D. V. Kent, and J. A. van Couvering (1985), Neogene geochronology and chronostratigraphy, in *Geochronology and the Geologic Time scale*, edited by N. J. Snelling, pp. 211–260, Geol. Soc., London.

Berggren, W. A., D. V. Kent, C. C. Swisher, and M.-P. Aubry (1995), *A Revised Cenozoic Geochronology and Chronostratigraphy*, *Spec. Publ. 54*, 212 pp., Soc. for Sediment. Geol., Tulsa, Okla.

Betzler, C., D. Kroon, and J. G. Reijmer (2000), Synchroneity of major late Neogene sea level fluctuations and paleoceanographically controlled changes as recorded by two carbonate platforms, *Paleoceanography*, *15*, 722–730.

Billups, K. (2002), Late Miocene through early Pliocene deep water circulation and climate change viewed from the sub-Antarctic South Atlantic, *Palaeogeogr. Palaeoclimatol. Palaeoecol.*, *185*, 287–307.

Bolli, H. M., et al. (1978), *Initial Reports of the Deep Sea Drilling Project*, vol. 40, 1079 pp., U.S. Govt. Print. Off., Washington, D. C.

Cepek, M., W. Brückmann, W. W. Hay, E. Söding, V. Spiess, J. Thiede, R. Tiedemann, and G. Wefer (1999), Integrated chronostratigraphy for DSDP/ODP drillsites in the South Atlantic Ocean, Ocean Drill. Stratigr. Network, Bremen, Germany.

Christensen, B., J. L. Kalbas, M. Maslin, and R. W. Murray (2002), Paleoclimatic changes in southern Africa during the intensification of Northern Hemisphere glaciation: Evidence from ODP Leg 175 Site 1085, *Mar. Geol.*, *180*, 117–131.

Davies, T. A., W. W. Hay, J. R. Southam, and T. R. Murray (1977), Estimates of Cenozoic oceanic sedimentation rates, *Science*, *197*, 53–55.

Dickens, G. R., and R. M. Owen (1999), The latest Miocene-early Pliocene biogenic bloom: A revised Indian Ocean perspective, *Mar. Geol.*, *161*, 75–91.

Diekmann, B., M. Faelker, and G. Kuhn (2003), Environmental history of the south-eastern South Atlantic since the middle Miocene: Evidence from the sedimentological records of ODP Sites 1088 and 1092, *Sedimentology*, *50*, 1–19.

Diester-Haass, L., and R. Zahn (1996), The Eocene-Oligocene transition in the Southern Ocean: History of water masses, circulation, and biological productivity inferred from high resolution records of stable isotopes and benthic foraminiferal abundances (ODP Site 689), *Geology*, *26*, 163–166.

Diester-Haass, L., and R. Zahn (2001), Paleoproductivity increase at the Eocene-Oligocene climatic transition and its role in the global carbon cycle: ODP/DSDP Sites 763 and 592, *Palaeogeogr. Palaeoclimat. Palaeoecol.*, *172*, 153–170.

Diester-Haass, L., P. A. Meyers, and P. Rothe (1990), Miocene history of the Benguela Current and Antarctic ice volumes: Evidence from rhythmic sedimentation and current growth across the Walvis Ridge (DSDP Sites 362 and 532), *Paleoceanography*, *5*, 685–707.

Diester-Haass, L., P. A. Meyers, and P. Rothe (1992), The Benguela Current and associated upwelling on the southwest African margin: A synthesis of the Neogene-Quaternary sedimentary record at DSDP sites 362 and 532, in *Upwelling Systems: Evolution Since the Early Miocene*, edited by C. P. Summerhayes, W. L. Prell, and K.-C. Emeis, pp. 331–342, Geol. Soc., London.

Diester-Haass, L., P. A. Meyers, and L. Vidal (2002), The Late Miocene onset of high productivity in the Benguela upwelling area as part of a global pattern, *Mar. Geol.*, *180*, 87–103.

Emeis, K.-C., J. W. Morse, and L. L. Mays (1991), Organic carbon, reduced sulfur, and iron in Miocene to Holocene upwelling sediments from the Oman and Benguela upwelling systems, *Proc. Ocean Drill. Program Sci. Results*, *117*, 517–527.

Exon, N. F., et al. (2001), *Proceedings of the Ocean Drilling Program, Initial Reports*, vol. 189, 98 pp., Ocean Drill. Program, College Station, Tex.

Farrell, J. W., I. Raffi, T. R. Janecek, D. W. Murray, M. Levitan, K. A. Dadey, K.-C. Emeis, M. Lyle, J.-A. Flores, and S. Hovan (1995), Late Neogene sedimentation patterns in the eastern equatorial Pacific, *Proc. Ocean Drill. Program Sci. Results*, *138*, 717–756.

Frank, M., N. Whiteley, S. Kasten, J. R. Hein, and K. O'Nions (2002), North Atlantic Deep Water export to the Southern Ocean over the past 14 Myr: Evidence from Nd and Pb isotopes in ferromanganese crusts, *Paleoceanography*, *17*(2), 1022, doi:10.1029/2000PA000606.

Froelich, P. N., et al. (1991), Biogenic opal and carbonate accumulation rates in the subantarctic South Atlantic: The late Neogene of Meteor Rise Site 704, *Proc. Ocean Drill. Program Sci. Results*, *114*, 515–550.

Gerhardt, S., and R. Henrich (2001), Shell preservation of Limacina inflata (pteropoda) in surface sediments from the central and South Atlantic Ocean: A new proxy to determine the aragonite saturation state of water masses, *Deep Sea Res. Part I*, *48*, 2051–2071.

Giraudeau, J., P. A. Meyers, and B. A. Christensen (2002), Accumulation of organic and inorganic carbon in Pliocene-Pleistocene sediments along the SW African margin, *Mar. Geol.*, *180*, 49–69.

Grant, K. M., and G. R. Dickens (2002), Coupled productivity and carbon isotope records in the southwest Pacific Ocean during the late Miocene-early Pliocene biogenic bloom, *Palaeogeogr. Palaeoclimatol. Palaeoecol.*, *187*, 61–82.

Gupta, A. K., and E. Thomas (1999), Latest Miocene - Pleistocene productivity and deep-sea ventilation in the northwestern Indian Ocean (Deep Sea Drilling Project Site 219), *Paleoceanography*, *14*, 62–73.

Haq, B. U., J. Hardenbol, and J. Hardenbol (1987), Chronology of fluctuating sea level since the Triassic, *Science*, *235*, 1136–1167.

Hart, T. J., and R. T. Currie (1960), The Benguela Current., *Discovery Rep*, *31*, 123–298.

Hay, W. W., and J. C. Brock (1992), Temporal variation in intensity of upwelling off southwest Africa, in *Upwelling Systems: Evolution Since the early Miocene*, edited by C. P.

Summerhayes, W. L. Prell, and K.-C. Emeis, pp. 463–497, Geol. Soc., London.

Hay, W. W., et al. (1984), *Initial Reports of the Deep Sea Drilling Project*, vol. 75, 1303 pp., U.S. Govt. Print. Off., Washington, D. C.

Herguera, J. C. (2000), Last glacial paleoproductivity patterns in the eastern equatorial Pacific: Benthic foraminifera records, *Mar. Micropaleontol.*, *40*, 259–275.

Herguera, J. C., and W. A. Berger (1991), Paleoproductivity from benthic foraminifera abundance: Glacial to postglacial change in the west-equatorial Pacific, *Geology*, *19*, 1173–1176.

Hermoyian, C. S., and R. M. Owen (2001), Late Miocene-early Pliocene biogenic bloom: Evidence from low-productivity regions of the Indian and Atlantic Oceans, *Paleoceanography*, *16*, 95–100.

Hodell, D. A., R. H. Benson, D. V. Kent, A. Boersma, and K. Racic-El Bied (1994), Magnetostratigraphic, biostratigraphic, and stable isotope stratigraphy of an upper Miocene drill core from the Sale Briqueterie (northwestern Morocco): A high resolution chronology for the Messinian stage, *Paleoceanography*, *9*, 835–855.

Hodell, D. A., R. Gersonde, and P. Blum (2002), Leg 177 synthesis: Insights into Southern Ocean paleoceanography on tectonic to millennial timescales, *Proc. Ocean Drill. Program Sci. Results*, 177, 1–54. (Available at http://www-odp.tamu.edu/publications/177_SR/VOLUME/SYNTH/SR177SYN.PDF.)

Hsü, K. J., and R. Wright (1985), History of calcite dissolution of the South Atlantic Ocean, in *South Atlantic Paleoceanography*, edited by K. J. Hsü and H. J. Weissert, pp. 149–187, Cambridge Univ. Press, New York.

Kennett, J. P. (1995), A review of polar climatic evolution during the Neogene, based on the marine sediment record, in *Paleoclimate and Evolution With Emphasis on Human Origins*, edited by E. Vrba et al., pp. 49–64, Yale Univ. Press, New York.

King, T. A., W. G. Ellis, D. W. Murray, N. J. Shackleton, and S. Harris (1997), Miocene evolution of carbonate sedimentation at the Ceara Rise: A multivariate data/proxy approach, *Proc. Ocean Drill. Program Sci. Results*, *154*, 349–365.

Krijgsman, W., F. J. Hilgen, I. Raffi, F. J. Sierro, and D. S. Wilson (1999), Chronology, causes and progression of the Messinian salinity crisis, *Nature*, *400*, 652–655.

Lange, C. B., and W. H. Berger (1993), Diatom productivity and preservation in the western equatorial Pacific: The Quaternary record, *Proc. Ocean Drill. Program Sci. Results*, *130*, 509–523.

Lange, C. B., W. H. Berger, H.-L. Lin, and G. Wefer (1999), The early Matuyama diatom maximum off SW Africa, Benguela Current System (ODP Leg 175), *Mar. Geol.*, *161*, 93–114.

Larsen, H. C., et al. (1994), Seven million years of glaciation in Greenland, *Science*, *264*, 952–955.

Laskar, J., F. Joutel, and F. Boudin (1993), Orbital, precessional, and insolation quantities for the earth from −20 Myr to + 10 Myr, *Astron. Astrophys.*, *270*, 522–533.

Lutjeharms, J. R., and P. L. Stockton (1987), Kinematics of the upwelling of southern Africa, *S. Afr. J. Mar. Sci.*, *5*, 35–49.

Lyle, M. (2003), Neogene carbonate burial in the Pacific Ocean, *Paleoceanography*, *18*(3), 1059, doi:10.1029/2002PA000777.

Lyle, M., K. A. Dadey, and J. W. Farrell (1995), The late Miocene (11–8 MA) eastern Pacific carbonate crash: Evidence for reorganisation of deep-water circulation by the closure of the Panama gateway, *Proc. Ocean Drill. Program Sci. Results*, *138*, 821–838.

Marlow, J. R., C. B. Lange, G. Wefer, and A. Rosell-Mele (2000), Upwelling intensification as part of the Pliocene-Pleistocene climate transition, *Science*, *290*, 2288–2291.

McRae, S. G. (1972), Glauconite, *Earth Sci. Rev*, *8*, 397–440.

Meyers, P. A., and Leg 75 Scientific Party (1983), Organic geochemistry of Benguela Upwelling sediments recovered by DSDP/IPOD Leg 75, in *Coastal Upwelling: Its Sediment Record, Part B*, edited by J. Thiede and E. Suess, pp. 453–466, Plenum, New York.

Molnar, P., P. England, and J. Martinod (1993), Mantle dynamics, uplift of the Tibetan Plateau, and the Indian Monsoon, *Rev. Geophys.*, *31*, 357–396.

Müller, G., and M. Gastner (1971), The "Karbonat-Bombe," a simple device for the determination of the carbonate content in sediments, soils and other materials, *Neues Jahrb. Mineral. Monatsh.*, *10*, 466–469.

Murray, D. W., and L. C. Peterson (1997), Biogenic carbonate production and preservation changes between 5 and 10 Ma from the Ceara Rise, western equatorial Atlantic, *Proc. Ocean Drill. Program Sci. Results*, *154*, 375–388.

Nees, S. (1997), Late Quaternary palaeoceanography of the Tasman Sea: The benthic foraminiferal view, *Palaeogeogr. Palaeoclimat. Palaeoecol.*, *131*, 365–389.

Oboh-Ikuenobe, F. (2001), A palynological record of middle Miocene to lower Pliocene sedimentary rocks, ODP Hole 1085A (Cape Basin, southwestern Africa) (abstract), *Eos Trans. AGU*, *82*(20), 228.

Ohkushi, K., E. Thomas, and H. Kawahata (2000), Abyssal benthic foraminifera from the northwestern Pacific (Shatsky Rise) during the last 298 kyr, *Mar. Micropal.*, *38*, 1–147.

Parker, F. L., and W. H. Berger (1971), Faunal and solution patterns of planktonic foraminifera in surface sediments of the South Pacific, *Deep Sea Res. Part A*, *18*, 73–107.

Paturel, J. (2000), Evolution des flux terrigenes dans le basin du Cap au Miocene superieur-Pliocene inferieur. Roles du systeme courantologique de Benguela et du climat africain, *Mem. DEA*, 45 pp., Univ. de la Mediterranee, Aix-Marseille II.

Peterson, L. C., D. W. Murray, W. U. Ehrmann, and P. Hempel (1992), Cenozoic carbonate accumulation and compensation depth changes in the Indian Ocean, in *Synthesis of Results From Scientific Drilling in the Indian Ocean, Geophys. Monogr. Ser*, vol. 70, edited by R. A. Duncan et al., pp. 311–333, AGU, Washington, D. C.

Peterson, R. G., and L. Stramma (1991), Upper-level circulation in the South Atlantic Ocean, *Progr. Oceanogr.*, *26*, 1–73.

Pickford, M., and B. Senut (1999), *Geology and Paleobiology of the Namib Desert, Southwestern Africa*, mem. 18., 155 pp., Geol. Surv. Namibia, Windhoek.

Prell, W. L., and J. E. Kutzbach (1992), Sensitivity of the Indian monsoon to forcing parameters and implications for its evolution, *Nature*, *360*, 646–650.

Ramsay, A. T. S., C. W. Smart, and J. C. Zachos (1998), A model of early to middle Miocene deep ocean circulation for the Atlantic and Indian Oceans, in *Geological Evolution of Ocean Basins: Results From the Ocean Drilling Program*, edited by A. Cramp et al., pp. 55–70, Geol. Soc., London.

Rea, D. K. (1992), Delivery of Himalayan sediment to the northern Indian Ocean and its relation to global climate, sea level, uplift, and seawater strontium, in *Synthesis of Results From Scientific Drilling in the Indian Ocean, Geophys. Monogr. Ser*, vol. 70, edited by R. A. Duncan et al., pp. 387–402, AGU, Washington, D. C.

Rea, D. K., I. A. Basov, L. A. Krissek, and Leg 145 Scientific Party (1995), Scientific results of drilling in the North Pacific transect, *Proc. Ocean Drill. Program Sci. Results*, *145*, 577–596.

Robert, C., and H. Chamley (1987), Cenozoic evolution of continental humidity and paleoenvironment, deduced from the kaolinite content of oceanic sediments, *Palaeogeogr. Palaeoclimat. Palaeoecol.*, *60*, 171–187.

Robinson, R. S., and P. Meyers (2002), Biogeochemical changes within the Benguela Current upwelling system during the Matuyama Diatom Maximum: Nitrogen isotope evidence from Ocean Drilling Program Sites 1082 and 1084, *Paleoceanography*, *17*(4), 1064, doi:10.1029/2001PA000659.

Rogers, J., and J. M. Bremner (1991), The Benguela ecosystem, part VII. Marine geological aspects, *Oceanogr. Mar. Biol. Ann. Rev.*, *29*, 1–85.

Roth, J. M., A. Droxler, and K. Kameo (2000), The Caribbean carbonate crash at the middle to late Miocene transition: Linkage to the establishment of the modern global ocean conveyor. *Proc. Ocean Drill. Program Sci. Results*, *165*. (Available at http://www-odp.tamu.edu/publications/165_SR/VOLUME/CHAPTERS/SR165_17.PDF)

Sancetta, C., L. Heusser, and M. A. Hall (1992), Late Pliocene climate in the southeast Atlantic: Preliminary results from a multi-disciplinary study of DSDP Site 532, *Mar. Micropaleontol.*, *20*, 50–75.

Schmiedl, G., and A. Mackensen (1997), Late Quaternary paleoproductivity and deep water circulation in the eastern South Atlantic Ocean: Evidence from benthic foraminifera, *Paleogeogr. Paleoclimat. Paleoecol.*, *130*, 43–80.

Schroeder, J. O., R. W. Murray, M. Leinen, R. C. Pflaum, and T. R. Janecek (1997), Barium in equatorial Pacific carbonate sediment: Terrigenous, oxide, and biogenic associations, *Paleoceanography*, *12*, 125–146.

Shackleton, N. J., and S. Crowhurst (1997), Sediment fluxes based on an orbitally tuned time scale 5 to 14 MA, Site 926, *Proc. Ocean Drill. Program Sci. Results*, *154*, 69–82.

Shackleton, N. J., and J. P. Kennett (1975), Late Cenozoic oxygen and carbon isotopic changes at DSDP Site 284: Implications for glacial history of the Northern Hemisphere and Antarctica, *Initial Rep. Deep Sea Drill. Project*, *29*, 801–807.

Shackleton, N. J., S. Crowhurst, T. Hagelberg, N. G. Pisias, and D. A. Schneider (1995), A new late Neogene time scale: Application to Leg 138 sites, *Proc. Ocean Drill. Program Sci. Results*, *138*, 73–101.

Shannon, L. V., and G. Nelson (1996), The Benguela: Large scale features and processes and system variability, in *The South Atlantic: Present and Past Circulation*, edited by G. Wefer et al., pp. 163–210, Springer-Verlag, New York.

Shipboard Scientific Party (1995), Site 925, *Proc. Ocean Drill. Program Initial Rep.*, *154*, 55–152.

Siedler, G., T. J. Müller, R. Onken, M. Arhan, H. Mercier, H. B. A. King, and P. M. Saunders (1996), The zonal WOCE sections in the South Atlantic, in *The South Atlantic: Present and Past Circulation*, edited by G. Wefer et al., pp. 83–104, Springer-Verlag, New York.

Siesser, W. G. (1978), Aridification of the Namib Desert: Evidence from oceanic cores, in *Antarctic Glacial History and World Paleoenvironments*, edited by G. J. van Zinderen-Bakker, pp. 105–112, A. A. Balkema, Brookfield, Vt.

Siesser, W. G. (1980), Late Miocene origin of the Benguela upwelling system off northern Namibia, *Science*, *208*, 283–285.

Summerhayes, C. P., D. Kroon, A. Rosell-Melé, R. W. Jordan, H.-J. Schrader, R. Hearn, J. Vilanueva, J. O. Grimalt, and G. Eglington (1995), Variability in the Benguela Current upwelling system over the past 70,000 years, *Progr. Oceanogr.*, *35*, 207–251.

Twichell, S. C., P. A. Meyers, and L. Diester-Haass (2002), Significance of high C/N ratios in organic-carbon-rich Neogene sediments under the Benguela Current upwelling system, *Org. Geochem.*, *33*, 715–722.

Van Andel, T. H., G. R. Heath, and T. C. Moore Jr. (1975), *Cenozoic History and Paleoceanography of the Central Equatorial Pacific Ocean: A Regional Synthesis of Deep Sea Drilling Project Data*, mem. 143, 143 pp., Geol. Soc. of Am., Boulder, Colo.

van der Zwaan, G. J., I. A. P. Duijnstee, M. den Bulk, S. R. Ernst, N. T. Jannink, and T. J. Kouwenhoven (1999), Benthic foraminifers: Proxies or problems? A review of paleoecological concepts, *Earth Sci. Rev.*, *46*, 213–236.

Verardo, D. J., P. N. Froelich, and A. McIntyre (1990), Determination of organic carbon and nitrogen in marine sediments using the Carlo Erba NA 1500 analyzer, *Deep Sea Res.*, *37*, 157–165.

Vidal, L., T. Bickert, G. Wefer, and U. Röhl (2002), Late Miocene stable isotope stratigraphy of Site 1085: Relation to Messinian events, *Mar. Geol.*, *180*, 71–85.

Vincent, E., J. S. Killingley, W. H. Berger (1985), *Miocene Oxygen and Carbon Isotope Stratigraphy of the Tropical Indian Ocean*, mem. 163, edited by J. P. Kennett, pp. 103–120, Geol. Soc. of Am., Boulder, Colo.

Wefer, G., W. H. Berger, C. Richter, and Shipboard Party (1998a), *Proceedings of the Ocean Drilling Program*, *Initial Reports*, vol. 175, 1477 pp., Ocean Drill. Program, College Station, Tex.

Wefer, G., W. H. Berger, C. Richter, and Shipboard Party (1998b), Facies patterns and authigenic minerals of upwelling deposits off southwest Africa, *Proc. Ocean Drill. Program Sci. Results*, *175*, 487–504.

Wise, S. W., et al. (1992), *Proceedings of the Ocean Drilling Program, Initial Reports*, vol. 120, 1155 pp., Ocean Drill. Program, College Station, Tex.

Woodruff, F., and S. M. Savin (1989), Miocene deep water oceanography, *Paleoceanography*, *4*, 87–140.

Wright, J. D., K. G. Miller, and R. G. Fairbanks (1991), Evolution of modern deep-water circulation. Evidence from the late Miocene Southern Ocean, *Paleoceanography*, *6*, 275–290.

Yasuda, H. (1997), Late Miocene-Holocene paleoceanography of the western equatorial Atlantic: Evidence from deep-sea benthic foraminifers, *Proc. Ocean Drill. Program Sci. Results*, *138*, 395–431.

Zachos, J., M. Pagani, L. Sloan, E. Thomas, and K. Billups (2001), Trends, rhythms, and aberrations in global climate 65 Ma to present, *Science*, *292*, 686–693.

T. Bickert, Fachbereich Geowissenschaften, Universität Bremen, D-28334 Bremen, Germany. (g05e@zfn.uni-bremen.de)

L. Diester-Haass, Zentrum für Umweltwissenschaften der Universität, Universität des Saarlandes, D-66041 Saarbrücken, Germany. (l.haass@mx.uni-saarland.de)

P. A. Meyers, Marine Geology and Geochemistry Program, Department of Geological Sciences, University of Michigan, Ann Arbor, MI 48109-1063, USA. (pameyers@umich.edu)